ANL-77-68

HIGH-PERFORMANCE BATTERIES FOR STATIONARY ENERGY STORAGE AND ELECTRIC-VEHICLE PROPULSION

Progress Report for the Period
April–June 1977

U of C-AUA-USDOE

ARGONNE NATIONAL LABORATORY, ARGONNE, ILLINOIS

Prepared for the U. S. DEPARTMENT OF ENERGY
under Contract W-31-109-Eng-38

Printed in the United States of America
Available from
National Technical Information Service
U. S. Department of Commerce
5285 Port Royal Road
Springfield, Virginia 22161
Price: Printed Copy $6.00; Microfiche $3.00

Distribution Category:
Energy Storage—Electrochemical
(UC-94c)

ANL-77-68

Argonne National Laboratory
9700 South Cass Avenue
Argonne, Illinois 60439

HIGH-PERFORMANCE BATTERIES FOR STATIONARY ENERGY STORAGE AND ELECTRIC-VEHICLE PROPULSION

Progress Report for the Period
April—June 1977

P. A. Nelson	Director, Energy Storage
N. P. Yao	Associate Director, Energy Storage
R. K. Steunenberg	Manager, Lithium/Metal Sulfide Battery Program
A. A. Chilenskas	Manager, Battery Commercialization
E. C. Gay	Section Manager, Battery Engineering
J. E. Battles	Group Leader, Materials Development
F. Hornstra	Group Leader, Battery Charging Systems
W. E. Miller	Group Leader, Industrial Cell and Battery Testing
M. F. Roche	Group Leader, Cell Chemistry
H. Shimotake	Group Leader, Cell Development and Engineering

October 1977

Previous Reports in this Series

ANL-76-81	April—June 1976
ANL-76-98	July—September 1976
ANL-77-17	October—December 1976
ANL-77-35	January—March 1977

PREFACE

The program on high-temperature secondary batteries at Argonne National Laboratory consists of an in-house research and development effort and subcontracted work by industrial laboratories. The work at Argonne is carried out primarily in the Chemical Engineering Division, with assistance on specific problems being given by the Materials Science Division and, from time to time, by other Argonne divisions. The individual efforts of many scientists, engineers, and technicians are essential to the success of the program, and recognition of these efforts is reflected by the individual contributions cited throughout the report.

TABLE OF CONTENTS

TABLE OF CONTENTS (contd)

LIST OF FIGURES

LIST OF TABLES

HIGH-PERFORMANCE BATTERIES FOR STATIONARY ENERGY STORAGE AND ELECTRIC-VEHICLE PROPULSION

Progress Report for the Period
April—June 1977

ABSTRACT

This report describes the research, development, and management activities of the program at Argonne National Laboratory (ANL) on lithium-aluminum/metal sulfide batteries during April-June 1977. These batteries are being developed for electric-vehicle propulsion and stationary energy storage. The present cells, which operate at 400-450°C, are of a vertically oriented, prismatic design with a central positive electrode of FeS or FeS_2, two facing negative electrodes of lithium-aluminum alloy, and an electrolyte of molten LiCl-KCl.

A major objective of this program is to transfer the technology to industry as it is developed, with the ultimate goal of a competitive, self-sustaining industry for the commercial production of lithium-aluminum/metal sulfide batteries. Technology transfer is being implemented by several means, including the assignment of industrial participants to ANL for various periods of time and the subcontracting of development and fabrication work on cells, cell components, and battery testing equipment to industrial firms.

Testing and evaluation of industrially fabricated cells is continuing. During this period, Li-Al/FeS and Li-Al/FeS_2 cells from Eagle-Picher Industries and from Gould Inc. have been tested. These tests provide information on the effects of design modifications and alternative materials for cells. Improved electrode and cell designs are being developed and tested, and the more promising designs are incorporated into the industrially fabricated cells. Among the concepts receiving major attention are carbon-bonded positive electrodes, scaled-up designs of stationary energy storage cells, additives to extend electrode lifetime, alternative electrode separators, and pellet-grid electrodes.

Materials development efforts included the development of a lightweight electrical feedthrough; studies of various current-collector designs; investigation of powder separators; wettability and corrosion tests of materials for cell components; and post-operative examinations of cells. Cell chemistry studies were concerned with discharge mechanisms of FeS electrodes and with other transition-metal sulfides as positive electrode materials. In addition, voltammetric studies were conducted to investigate the reversibility of the FeS_2 electrode. On studies of advanced battery systems the use of calcium and magnesium alloys for the negative electrode are being investigated.

SUMMARY

Commercial Development

A commercialization study was undertaken to assess the near-term markets for the following applications of the lithium/metal sulfide battery: vans, buses, mining vehicles, and defense uses. The results of this assessment indicate that the lithium/metal sulfide battery could enter these near-term markets, owing to its favorable performance characteristics.

The conceptual design/cost study for a 5.6 MW-hr truckable energy storage module is nearing completion. Also, systems design work was continued on the Mark 0 jacket for an electric-vehicle battery. This jacket is to be used as a housing for 50 cells in stationary testing.

In contractual work directed toward cell development, Catalyst Research Corp. completed the fabrication of an FeS_2 cell using their ultradry room for assembly; the negative electrodes were fabricated using a dip-casting procedure. Eagle-Picher Industries, Inc. is delivering FeS_x cells with modified cell designs (relative to baseline cells); the specific energy of these recent cells has been improved 10-20% over the previously delivered cells. Gould Inc. is in the process of fabricating a matrix of 55 upper-plateau FeS_2 cells, which cover a wide range of design variations. In addition, Gould Inc. is developing an improved design for the uncharged FeS cell.

In contractual work directed toward materials development, the production and stockpiling of boron nitride (BN) roving is proceeding at about 15 kg/month at Carborundum Corporation. Coors Porcelain is attempting to develop a brazed feedthrough that is resistant to chemical oxidation. ILC Technology is examining the kinetics of feedthrough failure in FeS_2 cells with sophisticated feedthrough designs. Chemetal is determining whether the vapor deposition of molybdenum onto substrates offers any advantages in the fabrication of current collectors.

Industrial Cell and Battery Testing

Two Eagle-Picher cells that incorporate changes from the baseline design of the FeS cell underwent testing. One of the new cells had its positive electrode half-thickness decreased from 6.0 to 4.2 mm and the ratio of negative-to-positive capacity increased from 1.00 to 1.33. The specific energy of this cell after 29 days of operation was 72 W-hr/kg at the 10 hr-rate, whereas that for the baseline cell was 62 W-hr/kg. The other modified cell had a positive electrode half-thickness of 5.6 mm and a negative electrode thickness of 6.6 mm; its negative-to-positive capacity ratio was 1.34. This cell has operated for 144 days and 238 cycles with only a 5% decline from its peak performance.

Two Eagle-Picher cells that incorporate changes from the baseline design of the FeS_2 cell underwent testing. One of these cells had the positive terminal rod moved from the center line of the cell to a position near one edge of the electrode (this position has some advantages in battery design). The results of this cell indicated a lower utilization of the active material. The other FeS_2 cell had a thinner and denser positive electrode and a larger negative plate than the baseline cell; this change increased the specific

energy from 67 to 72 W-hr/kg. This increase in specific energy was less than expected.

Studies have been directed toward current-limited, constant-voltage charging (CLCVC) with FeS and FeS_2 cells. A preliminary study of an FeS cell indicated that CLCVC does not significantly increase performance but does reduce charge time if high initial currents are used. Studies of two FeS_2 cells led to the following conclusions: (1) when the current limit is restricted to lower values, CLCVC is similar to constant-current charging, (2) constant-voltage charging is beneficial to cells that suffer some kinetic hindrance at the end of charge, and (3) CLCVC has no significant impact on cell lifetime.

Cells were tested in a series arrangement to study the interactions of the cells and to establish data for scale-up of battery designs. A two-cell battery, B7-S, has operated for more than 386 days and 595 (deep) cycles. During this period, the output energy of this battery (10-hr rate) has declined by 22% from its peak of 246 W-hr. A six-cell battery, B10-S, has had operating problems. One of its cells leaked electrolyte through its housing; this leakage caused electrical bridging around the mica sheets used for electrical insulation. The defective cell was replaced, but this new cell also leaked electrolyte. This cell was removed and a shim was used to replace it. Testing was then continued on the five-cell battery, designated B12-S.

Preparations are being made for laboratory testing of large-scale (30-60 kW-hr) batteries. In addition, design of an equalization charger has been completed; a power supply similar to the one that will go into the equalizer is being tested for performance characteristics. The system will have the capability of equalizing up to 104 cells at a rate of 0-12 A.

Three FeS cells and one FeS_2 cell with pellet electrodes have been constructed, and placed in operation.

Battery Charging Systems

A statement of work as a basis for a contract to perform a cost and design study of a complete charging system for a $LiAl/FeS_2$ electric-vehicle battery is now in the hands of a potential contractor. A "minicycler" has been modified by the addition of a constant-voltage, current-limiting circuit, and is performing well. An 100-ampere cell/battery cycler prototype was constructed, and final checkout is almost completed.

Cell Development and Engineering

One of the common reasons for cell failure is short circuits caused by extrusion of active material from the electrodes. Thus, in cell R-29 (an uncharged, upper-plateau $Li-Al/FeS_2-CoS_2$ cell) the positive electrode was reinforced with a double-strength frame. This cell has operated for 50 days without a decline in performance.

An upper-plateau, uncharged FeS_2 cell was built with X phase (Li_2FeS_2) as the starting material in the positive electrode. Excess lithium was added to the negative electrode in the form of Li-Al alloy plaques. After six

break-in cycles at a 5-A rate, this cell has a coulombic efficiency of 97% and a capacity of 72 A-hr (63% of theoretical).

Charged FeS_2-CoS_2 cells having hot-pressed electrodes and a separator/retainer material of Y_2O_3 felt are being tested to determine whether they produce high specific energy. One such cell, M-3, has operated for 90 cycles and 57 days. Although it is now showing signs of declining capacity, the coulombic efficiency was greater than 95% for 65 cycles. The specific energy of M-3 is 83 W-hr/kg at the 25-A discharge rate.

Carbon-bonded positive electrodes using FeS_2 as the active material continue to be investigated. Cell CB-1, a charged cell with a carbon-bonded $CuFeS_2$ electrode, has operated for 890 cycles and 503 days. The capacity of this cell has declined significantly over the last 100 cycles; the present capacity is 46 A-hr, which reflects a loss of 30% from peak capacity. An upper-plateau, carbon-bonded FeS_2-CoS_2 cell, KK-11, was operated for 50 days and 85 cycles before the test was terminated. The peak capacity of this cell was 71 A-hr; however, a furnace malfunction caused the capacity to decrease to 65 A-hr. The furnace malfunction also caused the coulombic efficiency to decrease by 3% (from 98 to 95%). Cell KK-10, an uncharged, upper-plateau FeS_2-CoS_2 cell, was fabricated in air using X-phase as the active material in the positive electrode. A Y_2O_3-felt particle retainer and a separator of new BN fabric were used in this cell. After 35 cycles, operation of this cell was terminated owing to declining coulombic efficiency. Examination showed that the BN fabric had disintegrated; the Y_2O_3 felt retainer appeared to be intact.

Small-scale experiments were undertaken to further define the optimum parameters for the preparation of carbon-bonded electrodes. The parameters investigated this period were pore volume and carbon content. The results showed a maximum utilization in the 25-35% pore volume range and in the 4-7 vol % carbon range.

Investigation is continuing on the addition of a third metal to the Li-Al alloy negative electrode in engineering-size cells. Cell FM-3, which has negative electrodes of Li-Al-8 wt % Sn, was operated for 232 cycles and 138 days; this cell exhibited very stable performance, with only a 10% decline in capacity after 200 cycles. The addition of tin to Li-Al alloy appears to enhance capacity over that of indium or calcium additive or no additive.

Three engineering-scale cells with ceramic-powder separators have been built and tested. The separators of PW-1 and PW-2 were 0.2 cm layers of Y_2O_3 powder. Cell PW-1 initially exhibited good performance; however, operation of this cell was terminated after 57 days and 116 cycles because of a short circuit. Cell PW-2 has operated for 25 days and 35 cycles, and has shown good performance. Cell PW-3 used a MgO-powder separator; performance of this cell was similar to that of the other two. This preliminary work shows powder separators to be promising.

Materials Development

For several years, all attempts to develop a brazed-seal feedthrough have resulted in premature failure owing to electrochemical oxidation and galvanic corrosion. To circumvent these problems, Coors Porcelain Co. has developed a

feedthrough with a nonmetallic braze and ILC Technology is investigating new feedthrough designs. After postoperative examinations of ANL crimp-type mechanical feedthroughs had indicated that little electrolyte salt penetrates into the BN seal, this feedthrough was redesigned to shorten the overall height to less than 2.56 cm.

The ability of BN fabric to retain the active materials within the electrodes was tested in a Li-Al/FeS cell. The electrodes were enclosed in metal frames with 200-mesh screens over the electrode faces; no additional particle retainers were used. This test cell showed excellent performance, and postoperative examination showed that the BN fabric was an effective particle retainer. Two powder separators were tested as alternatives to BN fabric. In the first, MgO powder was tested as a separator in a Li-Al/FeS cell. In similar fashion to the cell with a BN fabric separator, the electrodes were enclosed in metal frames with 200-mesh screens over the electrode faces. This test cell was operated for 83 days with good performance. Postoperative examination showed that, although the MgO powder was stable in this cell, impurities in the MgO powder were reduced to form a metallic band. Yttrium oxide powder was also tested as a separator in a Li-Al/FeS cell. No frames or screens were used around either electrode. This cell showed good performance at low current densities. The results suggested that the elimination of the frame and screen assembly around the positive electrode may be possible in cells with powder separators. The frame and screen assembly around the negative electrode appears to be needed.

Porous, monolithic separators are being prepared by die pressing and casting of foamed ceramic slips. A Y_2O_3 foam separator is being prepared for an in-cell testing. A mercury porosimeter has been received, and will be used to characterize the pore volumes and pore size distributions of candidate separator structures.

Static corrosion tests were conducted at 450°C in test environments of Cu_2S and CoS_2 in LiCl-KCl electrolyte. The following materials were evaluated: Hastelloy B, Inconel 625, Type 304 stainless steel, nickel, 1008 carbon steel (Cu_2S environment), and molybdenum (CoS_2 environment only). The results of these tests were then compared with those from previous tests on the same materials in FeS and FeS_2 environments. The corrosion resistance of the nickel-base material was about the same for both the Cu_2S and FeS environments; however, iron and its alloys were corroded more rapidly by the Cu_2S than the FeS. In the CoS_2 environment, the corrosion rates of the metals, with the exception of molybdenum, tended to be significantly higher than in an FeS_2 environment. These comparisons suggest that, under charged condition, FeS-Cu_2S electrodes with iron-base current collectors and FeS_2-CoS_2 electrodes with non-molybdenum components will have higher corrosion rates than similar electrodes without these metal sulfide additives.

A pretreatment process has been developed for BN separators that improves their wettability by LiCl-KCl electrolyte. This process involves the immersion of BN fabric in molten $LiAlCl_4$; after this is completed, the excess $LiAlCl_4$ is drained. Molten LiCl-KCl penetration tests have also been initiated on porous Y_2O_3 separators. These separators showed easy-to-penetrate behavior.

The vacuum system required for cell degassing experiments has been fabricated and attached to a quadrupole mass spectrometer. Testing of the system will begin after vacuum gauge installation is complete. In addition, a literature review has been completed on the ionic conductivity of molten LiCl-KCl eutectic and the theory of the conductivity of two-phase systems. This survey has provided the data necessary for estimating the electrical conductivity of electrolyte-separator combinations of interest to the battery program.

A review has been carried out concerning the causes of failure in prototype engineering cells that have undergone postoperative examinations over the last two years. Most of these cells were either operated until complete failure, or the test was terminated owing to declining performance. Short circuits have been the predominant cause of failure. The most common modes of failure have been extrusion of active material, separator cut by the honeycomb current collector, and metallic copper deposits within the separator. The cause for declining coulombic efficiency (partial short) has been attributed to a buildup of metal or metal sulfide deposits in localized areas within the separator, particularly in overcharged cells.

Cell Chemistry

Slow-scan cyclic voltammetry was used to study the FeS_2 electrode in a $LiAl/LiCl-KCl/FeS_2$ cell. The voltammograms showed that the discharge of FeS_2 was not kinetically hindered. On the other hand, the charge reaction was kinetically hindered, and required a combination of electrochemical and chemical steps to induce formation of FeS_2 from its precursors. The steps involve soluble sulfur species, as intermediates, that appear to be the source of sulfur (as Li_2S) in the separators of $LiAl/FeS_2$ cells. Additives to improve the charge kinetics of FeS_2 electrodes are now being sought.

A new phase was observed metallographically in partially discharged FeS_2 electrodes. This new phase, whose composition is yet to be determined, is the first discharge product of FeS_2 (earlier studies had indicated that the first product consisted of a mixture of $Li_4Fe_2S_5$ and $Fe_{1-x}S$). The new phase has been observed during both charge and discharge; however, FeS_2 does not appear to form readily from the new phase. More detailed studies of the properties of the new phase are in progress.

A study was conducted of three TiS_2 positive-limited electrodes that were pressed to about 70% theoretical capacity density. These electrodes varied in thickness from 0.20 to 0.66 cm. Good utilization was obtained at high rates even for the thickest electrode (76% utilization at 4-hr charge and 2-hr discharge rates). A sealed, 75 A-hr $LiAl/TiS_2$ cell was also operated, and achieved a specific energy of 67 W-hr/kg at the 10-hr rate.

Advanced Battery Research

The TiS_2, NiS, and $CuFeS_2$ positive electrodes were tested in small-scale calcium cells. Of these, NiS appears to have the best combination of reversibility, utilization, and resistance to overcharge. This positive electrode will be tested further in a 75 A-hr cell. Carbon current collectors were tested in iron sulfide electrodes to study their ability to control iron

oxidation in calcium cells. Neither of the two carbons tested (acetylene black and chopped graphite fibers) appeared to solve this problem.

A Mg-Al/FeS_2 and a Mg-Zn/FeS_2 cell showed good coulombic efficiency after a few weeks of operation. Studies of the Mg/FeS_2 system will be continued.

Cell and Battery Development at Atomics International

Small cells with Li_4Si negative electrodes, FeS positive electrodes, and LiCl-KCl electrolyte continue to be tested. Progress has been made toward optimization of powder separators in these cells. So far, AlN, Si_3N_4, and CaO powder have shown promise as a separator material.

I. INTRODUCTION

Lithium-aluminum/metal sulfide batteries are being developed at Argonne National Laboratory (ANL) for use as (1) power sources for electric vehicles, and (2) stationary energy storage devices for load-leveling on electric utility systems and storage of electrical energy produced by solar, wind, or other sources. Performance and lifetime goals for the electric vehicle batteries and stationary energy storage batteries are listed in Table I-1. These goals remain the same as those presented in the preceding report of this series (ANL-77-35, p. 9). However, future revision of these goals may be appropriate as the requirements of these two applications are investigated in greater detail through systems design studies.

Table I-1. Performance Goals for Lithium-Aluminum/Metal Sulfide Batteries

	Electric Vehicle Propulsion		Stationary Energy Storage	
Battery Goals	Mark I 1978	Prototype 1985	BEST 1982	Prototype 1985
Power				
Peak	30 kW	60 kW	1.5 MW	25 MW
Sustained Discharge	12 kW	25 kW	1 MW	10 MW
Energy Output	30 kW-hr	45 kW-hr	5 MW-hr	100 MW-hr
Specific Energy,[a] W-hr/kg	110	180	60-80	60-150
Discharge Time, hr	4	4	5	5-10
Charge Time, hr	8	5-8	8	10
Cycle Life	300	1000	1000	3000
Cost of Cells, $/kW-hr	-	35	25-30[b]	20

[a] Includes cell weight only; insulation and supporting structure is approximately 25% of total weight for the Mark I electric vehicle battery and 15 to 20% for the 1985 prototype vehicle battery.

[b] Projected cost at a production rate of 2000 MW-hr/yr.

Because the performance, cost, and lifetime requirements for the electric-vehicle and stationary energy storage applications differ significantly, separate approaches are being taken both in the conceptual design studies and in the development effort on cells and batteries for these two applications. The electric vehicle requires a battery of high energy and power per unit weight and volume to achieve the desired performance and range. The specific energy and power requirements are less severe for the stationary energy storage battery, but low cost and long lifetime are essential. The cells being developed for the electric-vehicle battery are relatively small, with individual capacities of about 150-200 W-hr. The cell design for the stationary energy storage battery is still in the conceptual stage. However, it is anticipated

that these batteries will consist of large, multielectrode cells having individual capacities of about 4-5 kW-hr.

The first in-vehicle test of a lithium/metal sulfide battery is scheduled for late 1978 or early 1979. This battery, designated Mark I, will have a capacity of about 30-40 kW-hr and will be tested in a van. A conceptual design of the Mark I battery has been completed and detailed design studies are in progress. Prior to fabrication of the Mark I battery, a preliminary test (Mark 0) will be conducted with a partial loading of cells in an insulated housing designed for the Mark I battery.

Conceptual design studies are nearly complete on a 5.6 MW-hr battery module for stationary energy storage applications. This design calls for the stacking of eight 4.4 kW-hr cells to form 35 kW-hr submodules. About 168 submodules would be loaded into a weatherproof insulated housing that can be shipped to the point of use by truck. The present plan is to test battery modules of this type in the BEST (Battery Energy Storage Test) Facility.

A study has been conducted on possible near-term (1980-1985) markets for lithium/metal sulfide batteries in which the cost requirements are less restrictive than for electric-vehicle or stationary energy storage applications. If lithium/metal sulfide batteries can be produced at a projected cost of $150/kW-hr in 1985, they could find a market as power sources for submersibles, postal vans, buses, and mining vehicles.

The battery development program consists of an in-house research and development effort at ANL and subcontracts with several industrial firms. The ANL effort includes cell chemistry studies, materials development and evaluation, cell and battery development, industrial cell and battery testing, and commercialization studies. Another small effort at ANL is directed toward the development of advanced battery systems that utilize low-cost, abundant materials. The major industrial subcontractors are the Atomics International Division of Rockwell International, Carborundum Co., Catalyst Research Corp., Eagle-Picher Industries, Inc., and Gould Inc. Atomics International is conducting a general research and development program with current emphasis on Li-Si/FeS cells for stationary energy storage batteries. The Carborundum Corp. is producing boron nitride fibers for electrode separators. Catalyst Research, Eagle-Picher, and Gould are involved primarily with the development and fabrication of cells that are tested either at ANL or in their own laboratories.

II. COMMERCIAL DEVELOPMENT
(A. A. Chilenskas)

The objective of the commercialization effort is to develop, with a minimum of federal support, a competitive self-sustaining industry capable of producing a supply of lithium/metal sulfide batteries that meets national needs. Commercialization planning has been undertaken to establish realistic technical and economic goals in meeting this objective. Important elements in our commercial development plan are the following: (1) materials and production costs for cells and assembled batteries, (2) marketing analyses, (3) manufacturing plans, and (4) analyses of competing systems and technologies.

A. Commercialization Studies
(S. H. Nelson*)

A rought draft of an assessment of the near-term (1980-1985) markets for various applications of the lithium/metal sulfide battery--vans, buses, mining vehicles, defense uses (*e.g.*, submersibles)--has been completed. This study† examines the potential of high-cost, low-volume markets for high-performance batteries.

In this assessment, the following battery performance characteristics were taken into consideration: specific energy, volumetric energy density, physical dimensions, service life, safety, maintainability, and compatibility with existing systems. In addition, the following four market characteristics were considered: ease of capture, status of competition, dates of markets, and applicable subsidies. The importance of each of these features to the various battery applications varied considerably; thus, separate estimation approaches were required for each application.

The defense and mining markets were evaluated by determining what kind of battery could meet the job specifications at a lower cost. For the van and bus markets, a comparison was made between the economic competitiveness of electric and conventional vehicles. This comparison was done without any consideration of the social benefits of electric vehicles (less noise, reduced pollution, etc.). A key assumption in this analysis is that time-of-day pricing, which has been mandated in at least six states, is practiced. This pricing scheme provides low rates for off-peak electric power (1-3¢/kW-hr).

1. Buses

In recent years, about 5000 conventional-type buses per year have been sold.[1] Projections through 1980 indicate that this sales level will remain fairly stable. Most of the bus companies are operated by municipal governments; and, although there are nearly 1000 bus systems, slightly over 50% of the buses are owned by the 20 largest systems. Thus, this market is

---

*Energy and Environmental Systems Division of ANL.

†Based upon information provided by L. Chrzanowski (Gould Inc.), R. Farmer (Eagle-Picher Industries, Inc.), and J. Von Osdol (Atomics International Division of Rockwell International). In addition, information generally available to the battery industry was used.

fairly concentrated. More than 60% of bus usage is for local routes with five or more stops per mile. These buses travel nearly 160 km/day (100 miles/day) and average 16-19 km/hr (10-12 mph). These conditions are suitable for electric buses with advanced batteries.

The principal competition for this market is the diesel bus, which costs about $75,000 and lasts 12 to 14 years.[2] These buses average 14 km/L (3.5 mpg) and have maintenance costs* of 14¢/km (23¢/mile).[3] Comparable electric buses would cost about $90,000 and last 18 to 23 years.[3] They would require approximately 400 kW-hr for a 160 km (100 mile) range and a 5.2 kW-hr/mile electrical input from the grid.[4] Operation and maintenance costs are expected to be 10¢/km (16¢/mile).[3] A present-value analysis (ANL-77-35, p. 14) has indicated that an electric bus would be cheaper to operate than a diesel-fueled bus by about $400-2200/year.† Given this economic advantage over diesel buses, electric buses should capture 20-60% of the near-term market. It is expected that 1500 electric buses will be needed in 1985; the market size‡ for these buses would be 6.0×10^5 kW-hr/yr.

The Urban Mass Transportation Administration (UMTA) administers an 80% federal subsidy for bus purchases. To obtain a subsidy, the purchaser must satisfy the UMTA that a new bus type is either cost effective or has social benefits sufficiently great to outweight any increased costs. The electric bus appears to be both cost effective and socially beneficial.

2. Vans

The projected van market is large. The market for the near term is an estimated 3,300,000 battery-powered vans. If the lifetime of the vans is assumed to be 12 years, then this market is 30,000 per year.

Although the van market is highly diverse, some very large fleets exist. For example, AT&T has over 140,000 vans and the U. S. Postal Service over 115,000. At present, the Postal Service has over 300 electric-powered vans and another 750 on order. Preliminary data by the Postal Service from the operation of these vehicles indicate that they are economical. At present about 30,000 of their internal-combustion vehicles can be replaced by electrical ones. Since the lifetime of their electric vans is 6-8 years, there is a market for 5000 postal vans a year. The estimated market size for the early 1980s is 10^5 kW-hr/yr.

Estimates of the economics for the remainder of this market are difficult to determine, due to a paucity of information. Nevertheless, one study estimates that the electric van market will be 55,000 vehicles in 1985.[5] For a van using a 50 kW-hr battery, this market would require 3.3×10^6 kW-hr of plant capacity.

---

*Costs in 1976 dollars.

†Assuming 43,000 km (27,000 miles) driven per year, and the cost of diesel fuel at 40¢/gal and electric power at 1¢-2.5¢/kW-hr.

‡Total battery production capacity needed in a year.

3. Mining Vehicles

The market for batteries in mining vehicles is governed by the following performance characteristics: (a) volumetric energy density, (b) physical dimensions, (c) safety, and (d) ease of maintenance. The cramped conditions underground and the attendent health hazard are responsible for these requirements.

The market itself is concentrated, with 75% of sales to three manufacturers. Because this market is dominated by so few manufacturers, market penetration involves very few decision makers. At present, lead-acid battery prices for mining vehicles range from \$110 to \$195/kW-hr with the average about \$140/kW-hr. Price increases are currently exceeding inflation.

The mining vehicle market is growing rapidly, with current demand at 1.9×10^5 kW-hr and the projected demand* for 1981 at 2.9×10^5 kW-hr. At the present growth rate, demand in 1985 would be 4.2×10^5 to 4.8×10^5 kW-hr. However, 25% of the above values are replacement batteries; and, because lithium/metal sulfide batteries require a new charger and replacement batteries do not, this portion of the market is probably not available for lithium/metal sulfide batteries. In fact, the potential market is even less than 75% of the total because new vehicles with lithium/metal sulfide batteries for already established mines would probably not be justified owing to the extra cost of a new charger. Thus, the available market for lithium/metal sulfide batteries may be as low as 10^5 kW-hr/yr in 1981.

4. Defense Applications

The possible defense applications of the lithium/metal sulfide battery are mobile launcher backup power in missile silos and propulsion of submersibles. Of these two, submersibles are the better prospect for the lithium/metal sulfide battery because the Department of Defense is interested in primary batteries, such as lithium/chlorine, for the silos.

The only decision maker in the battery market for submersibles is the Department of Defense. At present, silver/zinc batteries are being developed for this application. The cost goal for these batteries is \$333/kW-hr in 1983. In 1976 dollars, this value would be \$220/kW-hr at 5% yearly inflation and \$250/kW-hr at 6% yearly inflation. Our projected cost of the lithium/metal sulfide battery in 1983 is about \$200/kW-hr (1976 dollars). Thus, lithium/metal sulfide batteries for submersibles should be more economical than silver/zinc in the near term.

The total market size for nuclear submarines is estimated to be about 2.5×10^5 kW-hr. With a 2-year battery life (present requirement), the battery production needed is about 1.3×10^5 kW-hr/yr.

---

*Based upon mines under construction.

5. Conclusions

The results of this assessment indicate that several of the markets could support high-cost batteries for the near term. Although lithium/metal sulfide batteries may not completely capture these markets, they should be able to enter them, owing to their favorable performance characteristics. An estimate of the market size (total battery production capacity needed in a year) in 1985 for various battery applications is given in Table II-1.

Table II-1. Market Size[a] in 1985

Price, $/kW-hr	Market Size, kW-hr/yr	Applications of the Lithium/Metal Sulfide Battery
200	8.0×10^4-1.3×10^5	Submersibles
170	1.2×10^5-1.6×10^5	Postal vans
160	3.2×10^5-3.6×10^5	Postal vans and buses
150	9.6×10^5-1.1×10^6	Postal vans, buses, and mining vehicles

[a]Total battery production capacity needed in a year.

B. Systems Design
(A. A. Chilenskas)

The conceptual design/cost study for a 5.6 MW-hr, truckable energy storage module is nearing completion (see ANL-77-35, p. 15).

In a cooperative effort between Eagle-Picher Industries and ANL, a conceptual design of a jacket for a 30 kW-hr electric-vehicle battery has been completed; and a developmental phase is under way. This jacket (see ANL-77-17, p. 14), designated Mark 0, is designed to be used in thermal analysis studies of the vacuum-foil insulation and cooling/heating system. It is also planned to use this jacket as a housing for 50 cells in stationary testing as a preliminary engineering test prior to the development of the Mark I electric-vehicle battery. Fabrication of this jacket is scheduled for completion about November 1977.

C. Industrial Contracts

The contractual cell and battery development effort is directed toward (a) the transfer of technology from ANL research and development studies to the contractors and from contractor to contractor; (b) development of electrode designs, cell designs, and manufacturing techniques that can be used for load-leveling and electric-vehicle cells; and (c) development of hardware suited for large-scale manufacture in the future.

1. Cell and Battery Development Contracts
(R. C. Elliott, R. F. Malecha*)

Personnel from Catalyst Research Corp. participated in a technology transfer session at ANL. The emphasis of this meeting was concentrated on carbon-bonded positive electrodes. Catalyst Research believes that carbon-bonded positive electrodes would be ideally suited for fabrication in their plant. ANL is in the process of preparing the contractual documents to allow them to begin work in this area.

Catalyst Research completed the fabrication of an FeS_2 cell using their ultradry room (air atmosphere) for assembly. This cell has a positive electrode with a honeycomb current collector that was supplied by ANL. The negative electrodes were fabricated using a dip-casting procedure (developed by Catalyst Research) in which liquid Li-Al is cast onto a stainless steel screen in an inert-atmosphere glovebox. Operation of this cell should provide valuable information regarding the performance of this type of negative electrode and fabrication of charged cells in a dry air environment.

Eagle-Picher Industries, Inc. continued to deliver FeS and FeS_2 cells. The design of these cells has been modified from the baseline design by use of a cell design evaluation matrix. The results of the performance testing of these new cells are described in Section III.A. The specific energy of these recent Eagle-Picher cells has been improved 10-20% over that of the previously delivered cells.

During the quarter, ANL outlined in detail the effort required by Eagle-Picher for the balance of the calendar year. The areas that were outlined included: (1) the design and installation of a 500 ton (4.5×10^5 kg) press to produce 13 × 18 cm cold-pressed electrodes; (2) the fabrication of charged, upper- and two-plateau FeS_2 cells; (3) fabrication of new separator/retainer configurations as well as new positive electrode materials and additives; and (4) development of their cell test matrix.

The main thrust of the work at Gould Inc. is the fabrication of 55 upper-plateau FeS_2 cells. A cell test matrix has been devised to allow selection of the optimum set of design variables in these cells. Twenty-seven cells in this matrix cover a range of positive electrode thicknesses from 5.6 to 10.4 mm, porosities from 27 to 40%, and assumed negative-electrode utilizations of 65, 75, and 85%. The balance of the variations in cell design cover a range of current-collector candidates for the positive and negative electrode.

A product design review was held with Gould at ANL. The subject of this review was the 55-cell test matrix. As a result of this review, ANL requested that Gould proceed with the fabrication of six prototype cells across the matrix as soon as the contractual documents are processed. Completion of all the matrix test cells is expected in August, 1977.

Gould will have completed the installation of the salt filling and formation cycling equipment at their test facility in August.

---

*Chemical Engineering Division of ANL.

Another area of Gould's work is the continuing effort to develop an improved design for the uncharged FeS cell. Their primary goal is to improve the specific energy in FeS cells. A number of cells are being fabricated and tested at Gould under this program. Gould is also developing a multiplate cell design, which shows promise of delivering the highest specific energy of any FeS cell built to date.

The regular cell contractor update meeting was held at Eagle-Picher on June 2, 1977. Representatives from ANL, Catalyst Research, Gould, and Atomics International attended this meeting. A tour of the Eagle-Picher facility was included as part of the meeting.

2. Cell Materials and Component Development in Industry (J. E. Battles)

The production and stockpiling of boron nitride roving by the Carborundum Co. is proceeding at the rate of about 15 kg/month. The material is being stockpiled as roving for later conversion to either fabric or felt separators. Carborundum has continued development of BN-bonded felt separators (1.2 cm thick, 8% dense). A partial shipment has been received, and will be utilized in some of the cells fabricated by other industrial contractors. In addition, Carborundum has installed a fiber spinner for producing smaller-diameter BN fibers (0.5 to 2.0 μm *vs.* 6.0 to 8.0 μm). These fibers will be better suited for felt making and should considerably reduce the time for the first-stage nitriding (presently 86 hr). A preliminary cost estimate by Carborundum indicated a separator manufacturing cost of about $\$12.50/m^2$ ($\$1.25/ft^2$) at moderately high production rates. However, Carborundum indicated that considerable developmental effort remains to be done to optimize the felt fabrication process, to convert from a laboratory process to a production process, and to design a production plant.

Fiber Materials, Inc. has provided separator samples that were prepared using varying lengths of BN fibers with organic binders. The preliminary evaluations of these samples indicate that this approach to fabricating separators is unlikely to be successful. Thus, the remainder of the contract with Fiber Materials has been cancelled.

Coors Porcelain is attempting to develop a non-metallic, brazed feedthrough that is resistant to chemical oxidation. ILC Technology is examining sophisticated feedthrough designs. Both of these programs are discussed in greater detail in Section IV.A.1.

Chemetal is trying to determine whether or not the chemical vapor deposition of molybdenum onto base metal substrates offers any advantages in the fabrication of current collectors. Two areas were examined in this period: the fabrication of a molybdenum current collector with a copper conductor and the bonding of a conductor onto a molybdenum flat-sheet current collector. Some success was achieved in both areas, and samples for in-house evaluation are expected soon.

III. BATTERY ENGINEERING
(E. C. Gay)

Battery engineering includes (1) testing of industrially fabricated Li-Al/FeS_x cells and batteries assembled from these cells, (2) development of electrode and cell designs to meet the electric vehicle and stationary energy storage goals for cell performance, (3) improvement of cell-fabrication techniques, and (4) development of cells that use lower cost components. Statistical data on the FeS and FeS_2 cells operated over the past year are presented in Appendix A.

A. Industrial Cell and Battery Testing
(W. E. Miller)

1. Testing of Contractor-Produced Cells
(R. C. Elliott, P. F. Eshman, W. E. Miller, V. M. Kolba, G. W. Redding, J. L. Hamilton)

A performance summary of cells operated during the quarter is presented in Appendix B. Some of these cells are referred to as baseline cells, *i.e.*, they have been qualified by testing a series of cells with the same design to obtain baseline performance data. In later cells, design modifications were made, and the effects of these modifications were determined by comparing cell performance with the baseline data. For further discussion of Eagle-Picher Industries' baseline cells see ANL-76-98, pp. 15-17.

a. Eagle-Picher Baseline FeS Cells

Tests of baseline FeS cells with thin electrodes (Type A) fabricated by Eagle-Picher have not been reported previously. Although these cells are part of the original test grid, they were not subjected to qualification testing until recently. These cells have 3-mm-thick electrodes that are prepared by cold-pressing in an inert atmosphere glove box. The negative electrode composition is Li-Al (45 at. % Li); Cu_2S has been added to the positive electrode. Test results for one of these cells, EP-1A6, are presented in Table III-1; results of a baseline FeS cell with thick (6 mm) electrodes, EP-1B2, are presented for comparison. Owing to its lower weight, cell EP-1A6 showed a higher specific power than EP-1B2. The specific energy of EP-1A6 was greater than that of EP-1B2 at high discharge rates and lower at moderate discharge rates.

b. Eagle-Picher Modified FeS Cells

Eagle-Picher has delivered FeS cells with modified baseline designs. As compared with the Type 2B baseline cells, these new cells were thinner and lighter, and had higher negative-to-positive capacity ratios. In one of the new cells, EP-I-3-C-1, the ratio of negative-to-positive capacity was increased from 1.00 to 1.33 and the half-thickness* of the positive

*Because the cells have two negative electrodes and one positive electrode, the positive electrode is considered to consist of two halves. This dimension is referred to as the half-thickness.

Table III-1. Performance Data for Thick (Type B) and Thin (Type A) FeS Cells

Data	Baseline Cell EP-1A6 (Thin)	Baseline Cell EP-1B2 (Thick)
Average Coulombic Efficiency, %	96.99	99.98
Average Energy Efficiency, %	85.53	79.97
Discharge Cutoff Voltage, V	1.00	1.01
Charge Cutoff Voltage, V	1.60	1.62
Specific Energy, W-hr/kg		
At 2-hr rate	39	31
At 4-hr rate	46	44
At 10-hr rate	52	62
Peak Power,[a] W/kg (percent discharged)	52(5%)	29(5%)
Estimated Series Resistance,[b] mΩ	9.2	9.0

[a] 15-sec high-current pulse.

[b] 15-sec current interruption.

electrode was decreased from 6.0 to 4.2 mm. The specific energy of this cell after 29 days of operation was 72 W-hr/kg at the 10-hr rate and 50 W-hr/kg at the 4-hr rate. This is a significant improvement over the performance of the baseline cell.

The FeS cell EP-I-3-B-1 has a positive electrode half-thickness of 5.6 mm and a negative electrode thickness of 6.6 mm. Its loading ratio (negative-to-positive capacity) is 1.34. This cell has operated for 144 days and 238 cycles. Performance has been extremely stable, with only a 6% decline in performance since start-up. At the 4-hr rate (current density, 60 mA/cm^2), the specific energy is 46 W-hr/kg. At the 10-hr rate the specific energy is 60 W-hr/kg. Over the last 56 cycles, coulombic efficiency has declined only 3%.

c. Eagle-Picher Modified FeS_2 Cells

The first FeS_2 cells with designs modified from that of the FeS_2 baseline cells have been received from Eagle-Picher. One of the new designs (Type I-4) was similar to the Type 2B baseline cells except that the positive terminal rod was moved from the center line of the cell to a position near one edge of the electrode. (Battery design studies had previously indicated that this position of the positive terminal rod is the preferred one.) The negative electrodes contained a slightly greater Li-Al capacity loading than that of the baseline cell. Of the three Type I-4 cells delivered by Eagle-Picher, one (EP-I-4-1) has undergone qualification testing after 25 days of operation. These tests showed that the performance of EP-I-4-1 was poorer than that for a Type 2B baseline cell. For example, at a 4-hr rate, the specific energy of EP-I-4-1 was lower than that for a baseline cell, 50 *vs.*

67 W-hr/kg. The peak specific power was also lower (40 *vs.* 55 W/kg). The internal resistance (15-sec current interruption) was about the same in both cells. These results suggest a considerable lowering in utilization of the active material in the Type I-4 cells. This will be checked by qualification tests of cells EP-I-4-2 and -I-4-3.

Another of the cell designs, Type I-6, is similar to the Type 2B baseline cell except that it has a thinner and denser positive electrode and a larger negative plate. These modifications give a capacity loading of 1.27 (negative-to-positive ratio). The Type I-6 cell is thinner and lighter than its baseline cell. One of these cells, EP-I-6-A-1, has undergone qualification testing. This cell has a specific energy of 67 W-hr/kg, which is higher than that for the baseline cell. The peak specific power of this cell (57 W/kg) is also higher than that for the baseline cell.

2. Cell Heating and Cooling Experiments
(V. M. Kolba, G. W. Redding, J. L. Hamilton)

Investigation into the effects of charge-discharge current rates on the cell temperatures was continued (see ANL-77-35, p. 22) using the FeS_2 cell EP-2B6. Tests were conducted on the upper plateau with a discharge cutoff voltage of 1.25 or 1.50 V. The temperature variation during a discharge/charge cycle is given in Table III-2. Under these test conditions the average operating temperature was about 414°C, which is about 6°C lower than that previously found for a 10-A discharge and 5-A charge over the same voltage ranges. These lower temperatures suggest that battery temperature can be modified and controlled by the selection of discharge and charge conditions. This capability, coupled with a simple heating and cooling system, should permit control of battery operating temperatures within the 400 to 450°C range.

Testing of EP-2B6 has been terminated due to an inadvertent overcharge during set up and checkout of a new data acquisition system. The cell has been submitted to the Materials Group for postoperative examination (see Table IV-3).

Table III-2. Thermal Effect of Mixed Discharge and Charge Rates

Current, A		Cutoff Voltage, V		Temperature Change,[a] °C
Discharge	Charge	Discharge	Charge	
15	5	1.25	2.2	1.7
15	5	1.50	2.2	1.5

[a]Over a single cycle.

3. Charging Mode Studies

a. Charging of Cell EP-I-3-C-2
(V. M. Kolba, G. W. Redding, J. L. Hamilton)

The FeS cell, EP-I-3-C-2, is being used to compare a current-limited, constant-voltage charge (CLCVC) with a constant-current charge. A "mini-cycler" has been modified by W. W. Lark to permit charging at either constant current or current-limited constant voltage. The constant voltage charge may be set to current limits up to 25 A, after which the current is reduced as required to maintain the constant voltage. The constant voltage charge is terminated when a minimum (adjustable) current (*e.g.*, 2 A) is reached. All discharges are at a constant current.

The initial start-up and conditioning of EP-I-3-C-2 was at a 10-A constant current, with discharge and charge between 0.9 and 1.60 V. Comparison with EP-I-3-C-1, which was operated at constant-current charge, showed that the capacity of EP-I-3-C-2 was about 18% below that of -I-3-C-1. The reason for this is unknown. Changing from the 10-A constant-current charge to a 20-A CLCVC (decreasing to 2 A at end of charge) resulted in a 9% gain in energy on the next cycle. After two cycles the gain in energy reached ∿13.6%, but declined to ∿2.8% by the end of 11 cycles. A reduction in charging time of up to 32% occurred using the CLCVC.

After switching EP-I-3-C-2 from a 15-A CLCVC to a 15-A constant-current charge, the energy declined by about 9%, and remained fairly constant (within 1%) over the next 11 cycles. The 15-A CLCVC required about 30% more charging time than the constant-current charge but supplied only 7% more capacity. These preliminary results do not indicate a large benefit in performance with the CLCVC, but charge time is reduced with high initial currents.

b. Current-Limited, Constant-Voltage Charging
(R. C. Elliott)

Tests to determine the possible beneficial effects of various charging methods on the lifetime of cells are under way. These tests are being conducted with the computer-controlled Varien-Vidar-Robicon cell cycler. The first charging mode being examined is current-limited, constant-voltage charging (CLCVC). Ideally, this charging cycle consists of two parts. First, the current being delivered to the cell is limited to some constant value and the cell voltage is allowed to rise to the desired constant voltage limit. Second, after this constant voltage limit is reached, the current is reduced to maintain the constant voltage. In the charging tests, this new current, I_{new}, was calculated from the following equation:

$$I_{new} = I_{last} + \frac{E_o - E}{R_s}$$

where

I_{last} = previous current setting

E_o = constant voltage limit

E = observed voltage

R_s = series resistance

voltage limit. Descriptions of the batteries are given in Table III-3. A summary of battery performance data is given in Appendix C.

Table III-3. Description of Batteries

	Battery Designation			
	B7-S	B10-S	B11-S	B12-S
Cell Type[a]	FeS	FeS_2	FeS_2	FeS_2
Cell No.[b]	1B4, 1B6	I-5-1, 3, 4, 5, 7, 8	I-5-2, 3, 4, 5, 7, 8	I-5-3, 4, 5, 7, 8
Theoretical Capacity, A-hr	149	156	156	156
Total Operating Time				
Days	>386	36	52	>23
Cycles	>595	32	67	>34
Status	Operating	Terminated	Terminated	Operating

[a]All cells have Eagle-Picher thick electrodes.

[b]All cells fabricated by Eagle-Picher.

a. Two-Cell Battery Test

During this period, testing of FeS Cells EP-1B4 and -1B6 in series (designated Battery B7-S) was continued. With charge equalization, the performance of these two cells has declined significantly: at the 5-hr rate the specific energy was 23 W-hr/kg on cycle 570 and at the 10-hr rate it was 34 W-hr/kg on cycle 588. Without equalization, the capacity and energy at 10 A (initial rate, 10-hr) were higher than with equalization. For example, the specific energy on cycle 595 was 44 W-hr/kg, which is about 30% higher than the specific energy with equalization. This result will be verified by additional testing.

The battery has operated for more than 386 days and 595 cycles. Cell EP-1B4 in this battery has operated for more than 435 days and 629 cycles.

b. Six-Cell Battery Tests

Lithium/iron sulfide cells have been successfully tested as batteries in test chambers that were externally heated. The next phase of the program is to operate a battery in an insulated case. Thus, testing of Battery B10-S (six series-connected FeS_2 cells) in a vacuum-foil insulated case has begun. On the initial discharge cycle, increasing battery resistance (>111 mΩ) was observed. The battery was then cooled and removed from the case, and examination revealed oxidation of the copper bus bars at the bar-to-cell interfaces. The bus bars were cleaned and silver-plated at the contact areas of the cell leads and bus bars. The plug of the insulated case was modified to provide a purge line which extended to the rear of the battery package. The preoperation procedure was also modified: rather than relying on an inert

gas purge during heat-up and testing, evacuation and back filling of the case with inert gas was done prior to heat-up. These modifications appeared to have resolved the initial oxidation problems, as evidenced by subsequent testing.

The first of several cell failures to occur in this battery was that of Cell EP-I-5-1, which leaked electrolyte through pinholes in the cell housing. This leakage caused bridging around mica sheets used for electrical insulation of B10-S. This bridging created an electrical path between Cells EP-I-5-1 and -I-5-3, thus causing -I-5-3 to self-discharge to ∿0.25 V. Cell EP-I-5-1 was then replaced with EP-I-5-2 to form Battery B11-S. Cell EP-I-5-3 was individually charged prior to cycling of the battery in the test chamber. Start-up with the unconditioned cell intermixed with the cycled cells presented no problem. After resolving electronic and electrical problems, including replacement of the power supply, the battery was placed in the vacuum-foil insulated case. The initial discharge was within 1% of the capacity obtained in the test chamber. The battery resistance was about 68 mΩ. Near the end of the subsequent charge cycle, Cell EP-I-5-2 would not accept a charge. The battery was cooled down and examination showed that electrolyte had leaked around the positive lead of EP-I-5-2 and had subsequently bridged to the Conax feedthrough. The cell was removed from the cell stack and, since no similar cells were available, a spacer was used as a replacement. This assembly of five cells was designated B12-S.

Power input was measured during the testing of B10-S and B11-S. It was found that, during cycling, the required power to maintain the battery at ∿435°C was 50-53 W, which is about 12% less than indicated by previous data obtained from tests under static (no cycling) conditions.

c. Five-Cell Battery Tests

Operation of the five-cell battery, B12-S, has provided some interesting insights into battery operation. The initial cycle of B12-S yielded 19% more capacity and about the same energy as the last cycle of B11-S. The battery resistance was about 56 mΩ. Monitoring of individual cells limited discharge to 1.0 V and charge to 2.0 V. Equalization charging, when used, was to a limit of 1.95 V. After 11 cycles, the capacity, being limited by Cell EP-I-5-4, had declined to ∿61 A-hr. This cell was then removed from the limit-monitoring circuit and allowed to "float." On the subsequent discharge, the battery achieved a capacity of 87 A-hr and 78% of the initial energy. Near the end of discharge, Cell EP-I-5-4 was found to "reverse" to about -1.5 V (current, 7.5 A). On charging, this cell attained a maximum voltage of about 1.5 V. The average battery voltage was reduced by the loss of EP-I-5-2 and the differing voltage of EP-I-5-4 during cycling. On subsequent discharges at 10 A, the voltage of EP-I-5-4 did not reach values as negative as those when discharged at 7.5 A. Owing to progressive decline in capacity, on the 19th cycle Cell EP-I-5-7 was also taken off the monitoring system. Placing EP-I-5-7 on "float" brought about a temporary rise in capacity to 84 A-hr; however, with progressive cycling, the capacity again declined. Cell EP-I-5-7 did not "reverse" to the same extent as -I-5-4. The minimum battery voltage at the end of discharge is presently between 1.0 and 1.75 V.

The capacity and energy values obtained in B12-S are presented in Table III-4. When the average energy is very low and a battery voltage of

Table III-4. Performance of Battery B12-S

Cycle	Current, A	Capacity, A-hr	Energy, W-hr	Remarks
1	7.5	81	606	
13	7.5	87	473	EP-I-5-4 taken off monitoring system
19	10	63	431	
22	10	84	519	EP-I-5-7 taken off monitoring system

<1 V is reached, the battery will be shut down and its cells examined. Cell EP-I-5-4 will be especially interesting because we will be able to study the effects of voltage reversal.

5. Equipment for Electric-Vehicle Cell and Battery Tests
(V. M. Kolba, R. Alford,* W. E. Miller)

Static testing of 30-60 kW-hr batteries is scheduled for early 1978. Equipment, instrumentation, and support equipment will be specified, procured, installed, and checked out by February 1978. Our present plans call for simultaneous static testing of two electric-vehicle batteries. These will be cycled by a computer-controlled power supply to permit evaluation using driving profiles. The computer will also accumulate data at the end of each cycle. Cell monitoring, cycling mode selection, and other functions will be computer-controlled.

During this period, specifications for the power supply and the computer control and data-acquisition system were prepared, and procurement requests were initiated. In addition, a tentative proposal for control and distribution systems for the inert atmosphere in the battery case and the heating and cooling systems for the battery has been prepared.

A 2.7 × 6.6 m (9 × 22 ft) dry room (<300 ppm H_2O) is being planned for the following purposes: assembly of batteries, post-operative examinations, and repair of batteries that have electrolyte escaping from defective cells. In the latter case, low moisture levels are required to reduce corrosion by the exposed salt of the battery hardware and components.

Prototype bulk charge-equalizer systems for the electric vehicle will not be available for the static-test phase of the program. In lieu of this, an equalizer system for static battery testing is being procurred.

The design of the Mark 0-Mark I equalization system has been completed. A power supply similar to the one that will go into the equalizer is being tested for performance characteristics. Also, current-*vs.*-efficiency and voltage-*vs.*-efficiency curves will be run on this power supply to determine

*Industrial Particpant, Eagle-Picher Industries, Inc.

the feasibility of measuring the total power input to the system and calculating the power input into the cells. This would eliminate the need for measuring devices on the output of each supply.

The system will have the capability of equalizing up to 104 cells at a rate of 0-12 A. It will occupy a floor space of 0.8 m^2 (8 ft^2) and an overall height of 2.1 m (7 ft). Power supplies may be removed or replaced in the system in groups of two. Set-up of the voltage unit and current unit will be accomplished by plugging each supply into a "black box" that is able to simulate a cell; then the supply will be plugged back into the system. Construction is to begin in late July 1977.

6. Design and Testing of Pellet Cells

(R. Thompson,* P. F. Eshman)

Four baseline cells with pellet-grid electrodes have been constructed as described in ANL-77-35, p. 28. Cell PC-1-01 had a pellet-grid positive electrode of FeS-Cu_2S and a zirconia retainer next to both the positive and negative electrodes; the remainder of the cell consisted of standard FeS cell parts. Cell PC-2-01 was essentially identical to PC-1-01 except that graphite was added to the pellet and the zirconia retainer was next to the positive electrode only. Post-operative examination (see Section IV.A.8) of this cell indicated a possible short circuit caused by a chain of metallic particles that had moved out from the negative electrode through holes in the separator. The graphite was well confined to the positive electrode. In PNC-1-01, the Li-Al negative electrode had a pellet design, and, like PC-2-01, the zirconia retainer was next to the positive electrode. The remainder of this cell also consisted of baseline FeS cell parts. Cell PFC-1-01, a Li-Al/FeS_2-CoS_2 cell, was fabricated with a positive pellet grid. This cell was given a molybdenum grid structure similar in design to that used in the FeS pellet cells; the remainder of this cell consisted of baseline FeS_2 cell parts. Table III-5 presents a performance summary of all of the above cells.

Table III-5. Pellet Cell Performance

Cell No.	Lifetime		Utilization, %		Coulombic Efficiency, %		Energy Efficiency, %		Internal Resistance Range, mΩ
	Cycles	Days	Max	Final	Max	Final	Max	Final	
PC-1-01[a]	153	114	68.8	66.0	99.3	99.3	89.4	85.0	6.2-7.6
PC-2-01[a]	38	31	72.2	52.7	96.5	77.5	82.8	66.7	4.8-6.2
PNC-1-01[b]	41	41	80.0	73.6	96.5	87.9	78.4	73.4	8.0-8.6
PFC-1-01[a]	>19[c]	>20	77.4	65.7	99.4	93.4	87.4	72.9	9.4-14.7

[a]Current density, 44 mA/cm^2 (baseline cells operate at 31 mA/cm^2).

[b]Current density, 39 mA/cm^2.

[c]Cell still in operation.

*Industrial Participant from Gould Inc.

Some difficulty was encountered in welding the heavy molybdenum bus bar to the pellet grid in Cell PFC-1-01. Thus, an FeS_2 pellet cell is being fabricated that will use a minimal amount of molybdenum in the pellet-grid structure. The molybdenum grid for the design under consideration uses only 51% of the molybdenum required for the current collectors in the baseline FeS_2 cells (ANL-76-81, p. 12). This cell design is attractive from a cost viewpoint because molybdenum is very expensive.

B. Battery Charging and Control Systems

1. Charging Systems for the Electric-Vehicle Batteries
(F. Hornstra, W. H. DeLuca)

A statement of work as a basis for a contract to perform a design and cost study of a complete charging system for a $LiAl/FeS_2$ electric-vehicle battery is now in the hands of a potential contractor. A responsive proposal is expected by the end of July. This charging system is to provide automatically the main charge to the propulsion battery as well as the equalization charge to the cells. Size, projected cost, performance, and simplicity of operation are items that will be addressed in the study.

2. Electronics Development
(F. Hornstra, E. C. Berrill, W. W. Lark, C. A. Swoboda, J. M. Paul*)

A "mini-cycler" was modified by the addition of a constant-voltage, current-limited charging capability. This mode of operation allows the charging of a cell at a selected fixed current until a specified voltage is reached; the voltage then remains fixed as the current monotonically decreases to the self-discharge value. The charge cycle is automatically terminated when the current drops below a preset value. This method permits more charge to be returned to the cell than does the method of charging at a constant current until a voltage cut-off is reached. The modified minicycler has been operating stably and reliably in this mode for several weeks.

A quotation was solicited and received from Paraplegics, an outside fabricator, to construct an additional number of "mini cyclers" to meet the additional needs of the testing program.

A prototype 100 ampere cell/battery cycler has been constructed by the Electronics Division at ANL, and is in the final stages of checkout. This unit will cycle individual cells or a battery of up to four cells. Additional units will be produced when the prototype has been checked out. The subsequent interface of this cycler to a control computer has been explored. The unit was made to be remotely programmable; however, interface levels and logic conventions require specific consideration. Additional work remains to complete this definition.

---

*Electronics Division.

C. Cell Development and Engineering
(H. Shimotake)

The effort in this part of the program is directed toward improving the performance and lowering the cost of Li-Al/FeS_x cells. Technical advances resulting from this effort are incorporated into the cells that are fabricated by industrial firms. The present work is concentrated on the development of FeS_2 cells that are designed for operation on the upper-voltage plateau, with emphasis on high specific energy at high rates. Investigations are under way on (1) the prevention of short circuits in uncharged FeS_2 cells, (2) the assembly of uncharged FeS_2 cells in air using X-phase (Li_2FeS_2) as the starting material in the positive electrode, (3) the development of charged FeS_2 cells with advanced separator/retainer materials, (4) the development of carbon-bonded electrodes, and (5) the use of metal additives in cells with Li-Al electrodes. In addition, efforts are continuing on the scale-up of cells with advanced separators. A summary of performance data for the test cells is presented in Appendix B.

1. Uncharged Cells with Hot-Pressed Electrodes
(L. G. Bartholme and H. Shimotake)

One of the common causes for cell failure has been short circuits. These are usually caused by extrusion of active material from one electrode (owing to inadequate confinement) into the counter electrode. In Cell R-29, an uncharged, upper-plateau Li-Al/FeS_2-CoS_2 cell, the positive-electrode structure was reinforced with a double-strength frame to resist the expansion of the positive material. This cell has operated for 50 days and 100 cycles without a decline in capacity or coulombic efficiency.

We are continuing in our attempt to assemble an upper-plateau FeS_2 cell in air. Cell VB-3, a prismatic (13 × 13 cm) sealed cell, has been completely assembled in air. X-phase (Li_2FeS_2) was used as the active material in the positive electrode. The positive electrode was a hot-pressed Li_2FeS_2 plaque containing KCl as the binder. The negative electrodes consisted of pressed Al wire. Excess lithium was added to the negative electrodes in the form of thin lithium foil sheets that had been hot-pressed at 180°C under helium between thin aluminum sheets; these Li-Al alloy sheets had been sealed in aluminum foil under helium before the pressing of the electrode plaques. This technique avoids the contamination by gaseous impurities that normally results from the use of Li-Al powder. After six break-in cycles at 5-A charge and discharge, Cell VB-3 shows a coulombic efficiency of 97% and a capacity of 72 A-hr (63% of theoretical).

2. Charged Cells with Hot-Pressed Electrodes
(F. J. Martino, E. C. Gay)

Charged cells having hot-pressed electrodes and an advanced separator/retainer material of Y_2O_3 felt are being tested to determine whether they can produce high specific energy (>100 W-hr/kg). Lithium-aluminum alloy containing 55 at. % Li was used in the negative electrode, and hot-pressed FeS_2-10 mol % CoS_2 in the positive electrode.

Three such cells, M-1, M-2, and M-3, have been built and put into operation. All three cells were constructed in a similar fashion (see ANL-77-35, p. 31) with the following exceptions: (1) Cell M-2 weighed 360 g (or about 15%) less than M-1 owing to the fact that the current-collector straps of the negative electrode were a part of the cell housing; (2) the positive and negative electrodes of M-3 were half as thick (3 mm) as those of the other two cells; and (3) the Hastelloy B framework around the positive electrodes of M-1 and M-2 was replaced by molybdenum in M-3.

Cell M-1 showed good performance with a low resistance (2.7 to 4.8 mΩ). Its high average discharge voltage demonstrated the beneficial effect of the lithium rich Li-Al alloy in the negative electrode. Cell operation was terminated after 17 days owing to a rapid decline in coulombic efficiency.

Cell M-2 exhibited a similar performance to that of M-1. However, due to its reduced weight, M-2 had a small increase in specific energy over that of M-1, with values of 111 W-hr/kg at a 25-A discharge rate and 118 W-hr/kg at a 14-A discharge rate. The resistance of M-2 was low, 3.8 to 4.8 mΩ. After 31 cycles and 24 days of operation, testing of M-2 was also terminated because of a rapid drop in coulombic efficiency. Postoperative analysis showed that corrosion followed by the rupture of the Hastelloy B framework surrounding the positive electrode had pinched the Y_2O_3 felt separator/retainer material. This chain of events created a weakened area in the separator where a short circuit occurred.

The third cell in the series, M-3, has operated the longest, 90 cycles in 57 days. A schematic drawing of this cell is presented in Fig. III-2. Although now showing signs of decline, its coulombic efficiency was greater than 95% for 65 cycles. Cycling at the same discharge- and charge-cutoff voltages as the other two cells (1.18 and 2.18 V, respectively) M-3 has achieved a peak capacity of 73 A-hr (71% and 100% utilization of the negative and positive theoretical capacities, respectively). The specific energy of M-3 is 83 W-hr/kg at the 25-A discharge rate (current density, 92 mA/cm^2). Resistance ranges from 4.2 to 6.5 mΩ. Cell M-3 has a higher ratio of current collector weight to theoretical capacity than either M-1 or M-2. In spite of this, M-3 does not show improved electrode utilization over M-2 or M-1; and the peak power of M-3 at the 5-hr rate (25 A) is almost 30% less than that of M-2.

3. Carbon-Bonded Metal Sulfide Electrodes

(T. D. Kaun, W. A. Kremsner, F. J. Martino, W. Borger*)

Cell CB-1, an unsealed, charged cell of carbon-bonded chalcopyrite ($CuFeS_2$) and hot-pressed, pyrometallurgically prepared Li-Al is still operating after 890 cycles and 503 days. The capacity of this cell at the 5-hr rate (65 mA/cm^2) has declined significantly over the last 100 cycles. Lowering the charge current from 12.5 A to 8.0 A had little effect on regaining the lost capacity. The present capacity is 46 A-hr (31% of negative theoretical capacity), which reflects a loss of 30% from its peak capacity. The coulombic efficiency has remained at ∿97% and the resistance at 12 mΩ.

*Industrial Participant from Varta Batteries, A. G., Germany.

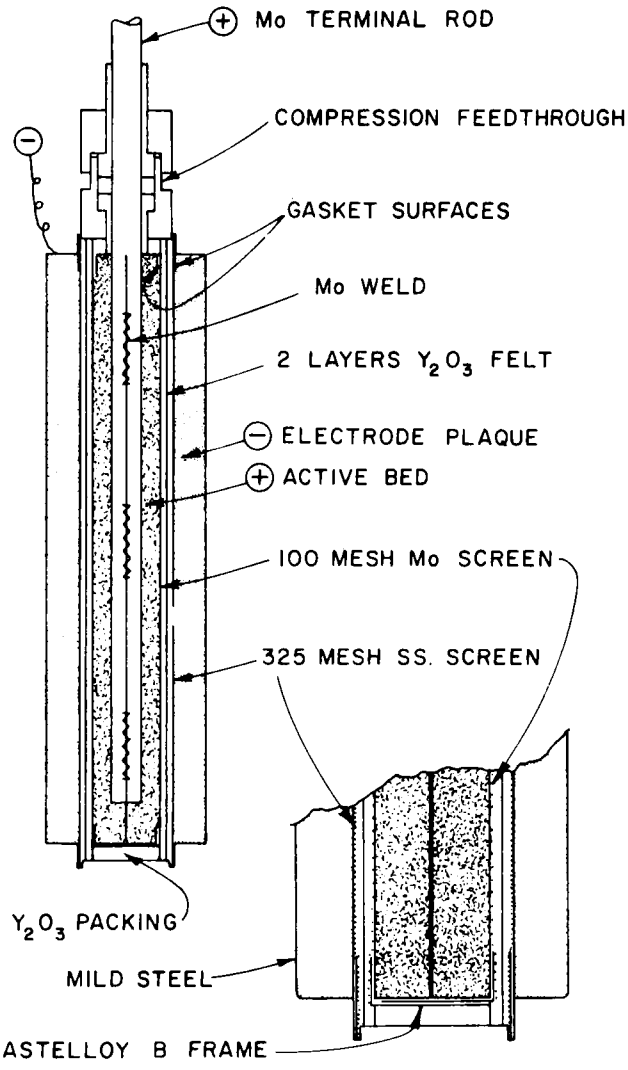

Fig. III-2. Schematic Drawing of Cell M-3

Cell KK-11, an upper-plateau, carbon-bonded FeS_2-CoS_2 cell, was built in a design similar to that of M-3 (see Fig. III-3). During start-up, KK-11 was inadvertently completely discharged to <0.7 V, and this may have changed the distribution of the active material in the positive electrode.

The peak capacity of KK-11 is 71 A-hr, with 25% on the lower-voltage plateau (this cell was designed as an upper-plateau cell). In spite of initial problems with this cell, KK-11 has performed well. After 26 days and 45 cycles, a peak power density of 180 W/kg was obtained at full charge and 100 W/kg at 50% discharge; resistance was 3.6 mΩ. At the 5-hr rate (current density, 51 mA/cm^2), the specific energy was 74 W-hr/kg with a 2.1-V charge cutoff. At the 2-hr rate (current density, 125 mA/cm^2), the specific energy was 63 W-hr/kg at a 1.0-V cutoff. At 35 cycles, a furnace malfunction increased the cell temperature to 500°C, and the coulombic efficiency decreased by 3% (from 98 to 95%) over the next 50 cycles. In addition, the capacity decreased from 71 to 65 A-hr and the resistance increased from 4.3 to 5.2 mΩ. Cell operation was terminated after 50 days and 85 cycles.

Cell KK-10, an uncharged, upper-plateau FeS_2-CoS_2 cell, was fabricated in air. X-phase (Li_2FeS_2) was used as the active material in the positive electrode. The negative electrodes consisted of pressed aluminum wire; excess lithium capacity was added through the use of a pressed Li-Al plaque encapsulated in aluminum foil (see Section III.C.1). The BN fabric used in the separator was a new material (smaller diameter yarn); a Y_2O_3-felt particle retainer was used in this cell. After 35 cycles, the cell was dismantled to determine the cause of low coulombic efficiency. Examination showed that the new BN fabric had disintegrated. Sections of the separator had completely disappeared; all that remained of the separator was loose fibers. The Y_2O_3-felt retainer appeared to be intact.

In connection with the preparation of X-phase material for the positive electrode of Cell KK-10, Li_2S and FeS powders were reacted at 1000°C for 4 hr in a graphite crucible to form a glassy black material. Photomicrographs by A. E. Martin revealed some Li_2S, FeS, and Fe. It was concluded that a more elaborate furnace with stirring capability was required to form large batches of X-phase. Exposing this X-phase to air for 48 hr produced a 60% weight gain. Analysis by B. Tani* showed no X-phase remaining; only hydrates with a small amount of FeS were present. Bulk X-phase material, therefore, should be handled in a dry room or inert atmosphere.

Small-scale experiments are being undertaken to further define the optimum conditions for the preparation of carbon-bonded (ANL-77-18, p. 15) electrodes. Two parameters being investigated are pore volume and carbon content, which can be varied over wide ranges. The effects of these two parameters on utilization are being determined in small, cylindrical FeS cells. The positive electrodes have a diameter of 6.25 cm and a capacity of 10 A-hr.

The results of these experiments showed that the utilization of the active material in these electrodes is strongly dependent on pore volume (see Fig. III-3).

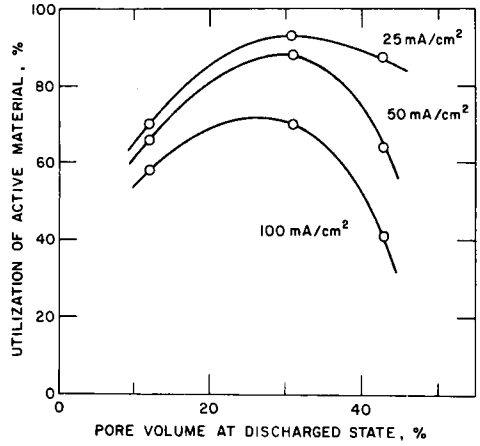

Fig. III-3.

Pore Volume of Carbon-Bonded FeS Electrode *vs.* Utilization of Active Material at 430°C

*Analytical Chemistry Laboratory of the Chemical Engineering Division at ANL.

The maximum utilization is obtained in the range of 25-35% pore volume (discharged state). At a low current density (25 mA/cm^2), utilization decreases only slightly at pore volumes greater than the maximum (>30%). On the other hand, at the higher current densities the utilization decreases very sharply at pore volumes greater than the maximum. For example, at 100 mA/cm^2, utilization drops from 70% at a pore volume of 31% to 41% at a pore volume of 43%. This effect is probably caused by an increase in resistance with increasing pore volume. In the region of low pore volume (about 13%), the drop in utilization with increasing current density is not very large; the utilization decreases from 70% at 25 mA/cm^2 to only 58% at 100 mA/cm^2. The diffusion of the Li^+ ions appears to be the capacity-limiting process in this region.

The utilization of the active material in these positive electrodes is also dependent on carbon content. The maximum utilization was observed at 4-7 vol % carbon. At carbon contents greater than this maximum, the utilization decreased with increasing carbon content.

4. Advanced Cell Design
(J. D. Arntzen)

Figure III-4 is a design for an upper plateau, uncharged cell (Cell A-4) with LiAl and FeS_2-CoS_2 electrodes. The objectives of this design were to provide edge support to the electrodes, eliminate void space, and reduce structural weight. Difficulty in achieving a good weld on the top of this cell required its operation as an open cell (this problem will be eliminated in the future). The specific energy* of this cell was 95 W-hr/kg at the 14-hr rate and 65 W-hr/kg at the 4-hr rate. These values were obtained in spite of a high resistance, about 13 mΩ. The testing of additional cells is planned to further examine the suitability of this design.

5. Cells with Li-Al Alloy Negative Electrodes with Additives
(F. J. Martino, H. Shimotake)

Engineering-size FeS cells (13 × 13 cm) are being operated to evaluate the effects of the addition of a third metal to Li-Al alloy electrodes. These cells have a negative electrode in which pyrometallurgically prepared Li-Al and an additive are loaded in an iron Retimet current collector.

The baseline cell with no additive, FM-0, has operated for 120 cycles in 62 days. Capacity has been about 52 A-hr at the 5-hr rate (60% utilization of negative theoretical capacity) with a discharge-charge current of 8 A (27 mA/cm^2). Cutoff voltages are set at 1.0 V for discharge and 1.70 V for charge. At present, there has been no decline in capacity or coulombic efficiency. Operation of Cell FM-3, which had negative electrodes of Li-Al-8.6 wt % Sn (86 A-hr theoretical capacity), was terminated after 232 cycles and 138 days. This cell demonstrated very stable performance, with only 10% decline in capacity after 200 cycles. In addition, during the first 100 cycles this cell's overall capacity was ∿10% higher than that of the baseline cell (FM-0).

*Calculation of this value included the weight of the cell top.

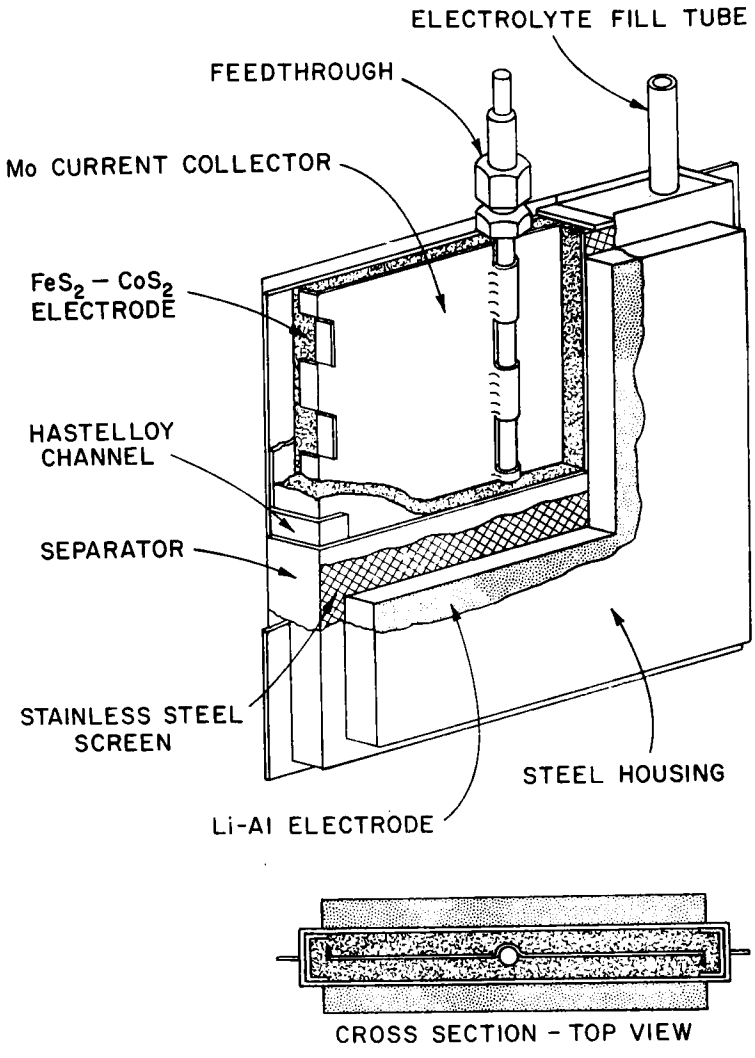

Fig. III-4. Advanced Design for Upper-Plateau FeS_2 Cell

The performance of FM-1 (indium additive) and FM-2 (calcium additive) was reported in ANL-77-35, p. 34. A summary of the performance of the FM-series cells is shown in Fig. III-5. As can be seen from this figure, the tin additive results in a higher capacity than indium additive, calcium additive, or no additive.

6. Cells with Advanced Separators
(T. W. Olszanski and H. Shimotake)

Three engineering-scale cells containing ceramic-powder separators have been built, and are being evaluated. These are the first scaled-up (12.4 × 13 cm) cells in which all-powder separators were used to replace the BN-fabric separator and zirconia-cloth particle retainer. Each cell was an upper-plateau FeS_2 type with approximately 120 A-hr capacity. All cells were made by a simple, two-step operation in which the separator and negative electrodes were hot pressed onto a pre-pressed positive electrode; the resulting

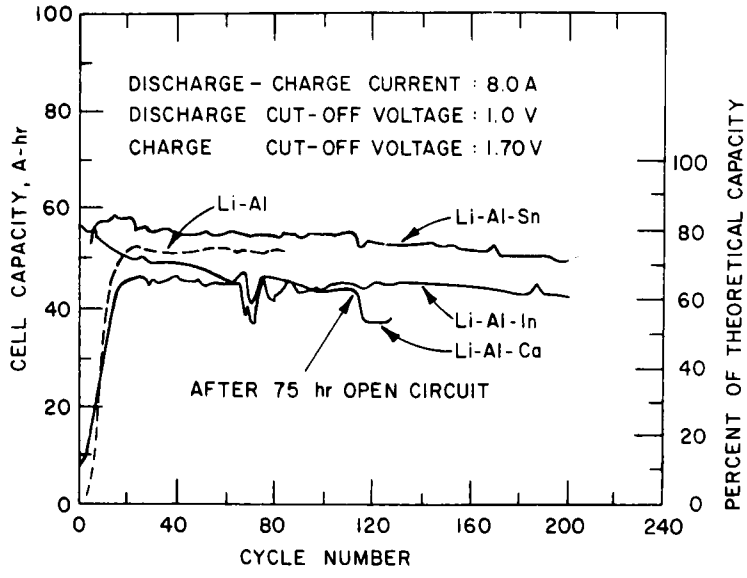

Fig. III-5. Cell Capacity *vs.* Cycle Number for FM Cells

plaque was placed in a can and sealed. The major advantages of the powder separator are low cost and ease of fabrication.

The separators of Cells PW-1 and PW-2 both were 0.2 cm layers of Y_2O_3 powder consisting of coarse particles (150-250 μm) that occupied 46% of the separator volume and fine particles (1-5 μm) that occupied 19% of the separator volume. LiCl-KCl electrolyte, acting as a binder, made up the balance of the separator. Both cells operated in an "electrolyte-starved" state.*

Operation of Cell PW-1 was terminated after 57 days and 116 cycles owing to a short circuit at the upper corner of the powder separator. The cell initially had high coulombic efficiency, and a 10 mΩ internal resistance. The electrolyte content, initially less than 300 g, was increased to 400 g because data had indicated that about 400 g of electrolyte was needed for PW-1 to reach optimum performance. Cell PW-2 has high coulombic efficiency and utilization, and has operated for 25 days and 35 cycles.

Cell PW-3 used a MgO-powder separator. This powder is much less expensive and less dense than Y_2O_3 powder. The MgO-powder separator consists of MgO particles (5-400 μm) that fill 70% of the separator volume; the remaining volume is LiCl-KCl electrolyte. Performance of this cell is similar to that of the previous powder cells. This cell has operated for over 6 days and 11 cycles, and is maintaining a high coulombic efficiency. A schematic drawing showing the design of the cells with ceramic powder separators is given in Fig. III-6.

*Cells typically contain excess electrolyte to ensure complete utilization of the active materials; the volume of electrolyte added to the "electrolyte starved" cell is restricted to that which can be absorbed within the separator and the electrodes.

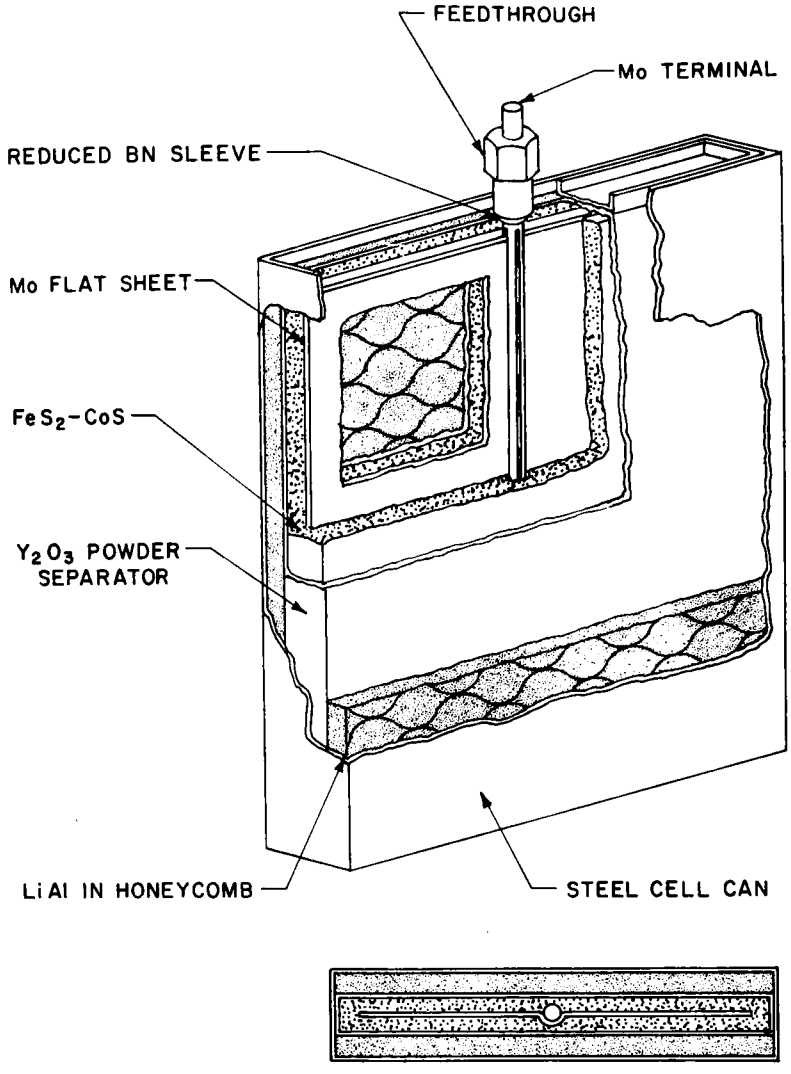

Fig. III-6. Schematic Diagram of PW Cells

An additional advantage of the powder separator is related to the type of feedthrough employed in the cell. Early results indicate that the BN sleeve of the feedthrough in a cell with a powder separator does not need to protrude into the electrode, as was the case with previous cells. The powder separator electrically insulates that portion of the feedthrough previously occupied by the BN sleeve. New feedthrough designs for powder-separator cells are under consideration by the Materials Group.

Thus far, the results for engineering-scale powder separator cells appear to be promising. Future efforts will focus on cell design and ways to optimize electrolyte content.

7. Performance Assessment of Upper-Plateau Cells
(H. Shimotake)

A number of tests involving upper-plateau FeS_2 cells were conducted in this quarter. Figure III-7 plots the specific energy *vs.* the current density for five of these cells. The shaded area represents the program's goals for the Mark I cell. As can be seen from this figure, the highly compact cells, such as M-1, and M-2, have met the specific energy goals for the Mark I cell in the region of low-to-moderate current density (<100 mA/cm^2). The less compact cells, such as R-24 and KK-11, are also very close to meeting these goals. In the high current density regions (>100 mA/cm^2), the specific energy goals have not yet been met.

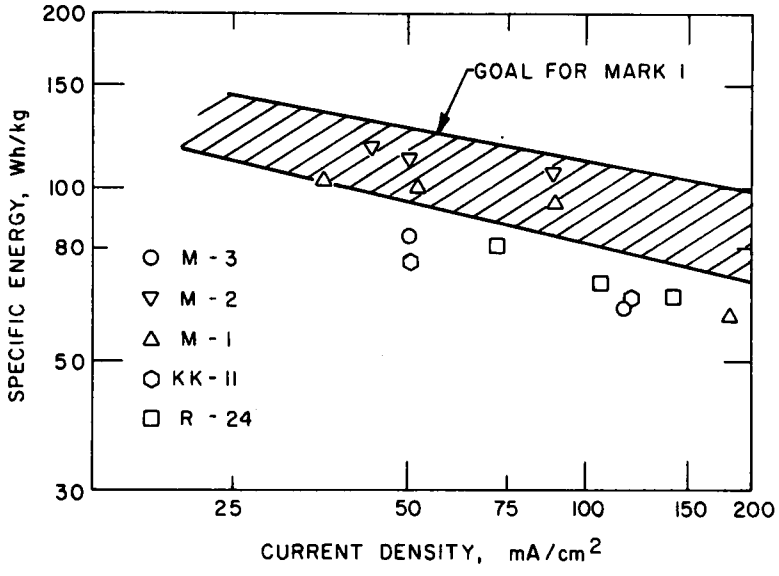

Fig. III-7. Specific Energy as a Function of Current Density of Upper-Plateau FeS_2 Cells

IV. TECHNOLOGY DEVELOPMENT

A. Materials Development
(J. E. Battles)

Efforts in the materials program are directed toward the development of various cell components (electrical feedthroughs, electrode separators, current collectors, and cell hardware), testing and evaluation of cell materials (corrosion and wettability testing), and postoperative examination of cells to evaluate the behavior of the electrodes and the construction materials.

1. Electrical Feedthroughs
(K. M. Myles and J. L. Settle)

The corrosive environment within Li-Al/LiCl-KCl/FeS_x cells precludes the use of any known electrical feedthroughs that are commercially available. The best long-term solution may be a braze-seal feedthrough, but to date no reliable ceramic-to-metal braze has been found. In the meantime, several mechanical-seal feedthroughs have been sufficiently refined to provide a temporary solution.

For several years, the effort to develop a brazed-seal feedthrough has involved two approaches. In the first, attempts were made to protect the brazed joints of conventionally metallized feedthroughs by coating the braze with corrosion-resistant metals. In-cell tests showed rapid failure because the coating could not adequately cover the exposed edge of the braze. The second approach involved the utilization of metals that were considerably less active than the usual braze alloys; these metals are less likely to be electrochemically oxidized during the charge cycle. Unfortunately, alloys that could be successfully brazed to the ceramic (BeO) also oxidized rapidly at potentials near the charge-cutoff voltage. The very short lifetimes of these feedthroughs make them unacceptable for cell use.

To minimize the possibility of chemical oxidation at the positive electrode during charging, a nonmetallic braze has been substituted for the metallic one. Coors Porcelain has produced preliminary test samples of Y_2O_3 that has been coated with several nonmetallic brazes. These samples have satisfactorily withstood exposure to the cell environment.

Several composites (two small sheets of molybdenum brazed onto opposite sides of a ring of Y_2O_3) were subjected to an in-cell corrosion test. In this test, an external potential was applied across a sample immersed in a beaker of molten LiCl-KCl electrolyte. The negative tab was connected to a LiAl reference electrode. The potential was maintained at 1.8 V, and the current through the sample was monitored. Within hours a short circuit developed across the ceramic. The composites were removed from the cell, immersed in methyl alcohol to dissolve any lithium, and then immersed in water to dissolve any salt. After this cleaning, the short circuit disappeared; the tabs were still firmly joined to the yttria. However, subsequent in-cell testing caused the short circuit to re-form. Aliquots of the cleaning solutions have been submitted for chemical analysis. Additional development work by Coors will be suspended until the failure mechanism is understood and a remedy is found.

Tests are underway at ILC Technology to establish specifications for feedthrough designs. ILC Technology is examining the effects of sophisticated design geometries on the kinetics of feedthrough failure for FeS_2 cells. One of their main concerns is to minimize the extent of corrosive attack on marginally corrosion-resistant, low-cost construction materials. This program will closely interact with a program sponsored by Atomics International and the Electric Power Research Institute at ILC to develop a feedthrough for FeS cells.

As described in ANL-77-17, pp. 32-33, several significant modifications have been incorporated into the ANL crimp-type mechanical feedthrough that have resulted in an improved design. In this period, after metallographic examinations demonstrated that only a very small amount of electrolyte salt penetrates into the BN seal of the ANL crimp-type feedthrough, the length of the seal was decreased from 12.8 to 9.6 mm. In addition, the height of the ceramic insulators was decreased to yield a total decrease of 12.8 mm in the length of the feedthrough. The resultant overall length of the feedthrough is less than 25.4 mm. The reduction in the size of the ceramic parts will result in decreased fabrication cost.

2. Electrode Separators
(J. P. Mathers and C. W. Boquist)

Paper, felt, and powder separators are being developed as alternatives to the BN fabric that is currently used as the electrode separator in Li-Al/LiCl-KCl/FeS_x cells. These candidate separators are expected to be considerably less expensive than BN fabric and to provide more effective retention of the active materials in the electrodes.

The ability of BN fabric to retain the active materials within the electrodes was tested in a cylindrical (7.5 cm-dia) Li-Al/FeS cell assembled in the discharged state. The electrodes were enclosed in metal frames with 200-mesh screens over the electrode faces; no additional particle retainers were used. This cell was cycled continuously at 60 mA/cm^2 for 52 days before its operation was voluntarily terminated. The electrical performance of the cell was excellent throughout operation. Postoperative examination showed that some of the active materials from the positive electrode had moved through the 200-mesh screen; however, most of this escaped material had been retained by the BN fabric. In a few locations, some active material had migrated into the fabric (in the interstices between the yarns), but the amount of active material at these locations was very low. These results suggest that BN fabric can be used as an electrode separator with no other particle retainers than screens over the electrode faces. Further testing in engineering-size cells will be required to confirm this finding.

A low cost (<$1/lb), MgO powder was tested in a cylindrical (7.5 cm dia) FeS cell assembled in the discharged state. The electrodes were enclosed in metal frames with 200-mesh screens over the electrode faces; no additional retainers were used. The MgO was packed into place around the positive electrode. The MgO was a mixture of 70 wt % fused MgO grain (-100 mesh)* and 30 wt % calcined MgO (-40 mesh).† The calcined MgO contained a large fraction

*General Electric Company, Type 12701-2X.

†Martin-Marietta Chemicals, Type 169.

of -200 mesh particles. This powder was added to the fused MgO grain to reduce the free flowing characteristics of the fused grain. The cell was cycled continuously for 83 days at a current density of 60 mA/cm^2. The coulombic efficiency was very good, although the utilization showed a gradual decline from 36 to 23% in the last 33 days of operation. Postoperative examination showed a comparatively large amount of a metallic phase in the lower third of the separator, adjacent to the negative electrode. The metallic phase contained Ca, Si, Al, and Mg. The as-received, fused MgO grain contained ~6% $Al_2O_3 \cdot CaO \cdot SiO_2$ impurity grains and a $CaO \cdot MgO \cdot SiO_2$ glass phase that was associated with many of the MgO particles. The non-MgO phases appeared to be reduced in the cell environment to form the metallic phases. The fused MgO grains were only slightly etched on the particle surfaces. Because of its fine particle size, the calcined MgO was difficult to resolve in micrographs; efforts to study its stability in the cell are continuing. The apparent stability of the fused MgO is encouraging, and work is in progress to evaluate other low cost MgO powders that contain fewer impurity phases.

During this period, the design for the separator test cell was changed from a cylindrical to a prismatic (7.6 × 12.7 cm) configuration. This new design will better simulate the conditions in an engineering cell. The first prismatic cell had a Y_2O_3 powder separator, and was assembled in the discharged state. The electrodes and separator were formed by hot-pressing, using the electrolyte as a binder. No frames or screens were used around either the positive or negative electrodes. A flat plate current collector was used in the center of the positive electrode, and the cell housing served as the current collector for the negative electrodes. This cell had very good electrical performance at low current densities (~20 mA/cm^2), but poor performance at higher current densities (60 mA/cm^2). The poor performance at high current densities is believed to have resulted from insufficient void volume and current collection in the negative electrodes. Postoperative examination revealed that the separator had remained in a fairly uniform band between the electrodes and had conformed to small dimensional changes in the electrodes. These results indicate that elimination of the frame and screen assembly around the positive electrode may be possible in cells using powder separators. The frame and screen assembly appears to be needed around the negative electrodes to aid in current collection. Elimination of the positive electrode frame would simplify cell design, reduce the cell weight, and eliminate the problem of finding a low cost frame and screen assembly that can withstand sulfide attack in FeS_2 cells.

3. Ceramic Materials

(W. D. Tuohig and J. T. Dusek)*

Porous, monolithic separators are being prepared by die pressing and by casting of foamed ceramic slips. Promising results were obtained by pressing calcined Y_2O_3 powder (1350°C) containing up to 18 wt % of an acrylic resin and stearic acid mixture. The organic materials were introduced in an excess of CCl_4 solvent that was subsequently evaporated. The resulting cake was then granulated and screened to size. Pressing the granulated powder at pressures of 7-15 MN/m^2 (1000-2000 psi) produced a compact that retained its granular structure after firing at 1500°C for 12 hr. Table IV-1 summarizes the Y_2O_3 separator structures generated by this technique.

*ANL Materials Science Division.

Table IV-1. Yttrium Oxide Separator Structures Prepared by Granulation

Specimen Number	Wt % Binder[a]	Particle Size Fraction[b]	Compaction Pressure, MN/m^2	Vol % Porosity
433D	12	-100	35	48
438A	18	-20 + 30	69	44
438B	18	-20 + 30	69	45
438C	18	-20 + 30	69	45
438D	18	-20 + 30	35	50
438E	18	-20 + 30	35	49
442A	18	-30 + 60	69	44
442C	18	-30 + 60	35	49
442D	18	-30 + 60	35	48
442E	18	-30 + 60	35	49
446A	18	-60 + 100	69	42
446B	18	-60 + 100	69	43
446C	18	-60 + 100	35	48
446D	18	-60 + 100	35	47
450A	18	-100	69	40
450B	18	-100	69	36
450C	18	-100	69	43
450D	18	-100	35	45
450E	18	-100	35	47
451A	12	-20 + 30	18	--
451B	12	-20 + 30	12	60
451C	12	-20 + 30	6	64
452A	12	-30 + 60	18	65
452B	12	-30 + 60	18	65
452C	12	-30 + 60	18	66
452D	12	-30 + 60	6	63
453A	12	-60 + 100	6	66
454A	12	-100	18	65
454B	12	-100	6	62
455A	18	-20 + 30	18	63
455D	18	-20 + 30	6	60
456A	18	-30 + 60	18	63
456B	18	-30 + 60	12	62
456C	18	-30 + 60	6	64
457A	18	-60 + 100	6	60
458A	18	-100	6	67

[a]Weight percent on a solid basis of 3:1 mixture of acrylic resin and stearic acid.

[b]U. S. Standard sieve sizes.

Foamed ceramic separators prepared by mechanical entrainment of air in an aqueous suspension of fine powders have been described previously (ANL-76-98, p. 34). Subsequently, foamed structures have been prepared with the aid of a commercial foam generator.* The generator produces a foam from air and an aqueous solution that can be combined with a ceramic slurry to produce foams of any predetermined density. These foams can be stabilized by reaction of the Y_2O_3 with weak nitric acid or by the gelation of water-soluble resin. The latter process is under investigation. Preliminary penetration tests with LiCl-KCl electrolyte (see Section IV.A.5) indicate that foam structures are readily infiltrated by the molten salt. Prototype full-scale separators are being prepared for cell testing.

A mercury porosimeter† has been received, and is being checked out. The instrument will be used to measure total pore volumes and pore size distributions of separator materials.

4. Corrosion Studies
(J. A. Smaga and K. M. Myles)

Current collectors in the positive electrode are exposed to metal sulfides and molten LiCl-KCl eutectic, a condition that results in rapid attack on most commonly used metals. Because of the importance of developing current collectors, a number of metals have been subjected to corrosion tests in equal-volume mixtures of both Cu_2S + LiCl-KCl and CoS_2 + LiCl-KCl at 450°C. (The test sulfides, Cu_2S and CoS_2, are representative of the additives to FeS and FeS_2 electrodes, respectively.) The following materials were evaluated: Hastelloy B, Inconel 625, Type 304 stainless steel, nickel, 1008 carbon steel (Cu_2S environment only), and molybdenum (CoS_2 environment only). The test results are summarized in Table IV-2, and include corrosion rates for materials studied previously in FeS and FeS_2 environments (ANL-77-17, p. 38).

For the samples evaluated in the Cu_2S environment, the corrosive attack was strongly dependent on whether the metal was an iron- or nickel-base material. The samples of low-carbon steel (1008 carbon steel) underwent complete reaction in less than 500 hr, and had corrosion rates greater than five times the rates found for low-carbon steel in the FeS environment. Type 304 stainless steel showed extensive intergranular attack. Deposition of metallic cooper on the stainless steel and especially the nickel-base materials masked the true weight losses of these samples. This effect prevented the determination of valid corrosion rates. The deposition layers covered from 10 to 80% of the sample surface area, and often reached thicknesses of 50 μm. However, the interface between the base metal and the deposition layer was easily discernable by metallographic examination; neither nickel nor Hastelloy B showed any appreciable base metal attack. Inconel 625, which contains up to 5 wt % Fe, did show areas of intergranular attack. Copper deposition was not restricted to the test samples. Deposits were found on the quartz test container and within the sulfide-salt environment. The ease of copper formation at cell operating temperatures may be a key in explaining the high content of copper particulate in the separators of cells employing FeS-Cu_2S electrodes.

*Model OJ-10-5, Mearl Corp., Roselle Park, NJ.

†Model 915-2, Micromeritics Instrument Corp., Norcross, GA.

Table IV-2. Corrosion Rates for Various Metal Sulfide Environments at 450°C

Material	Environment[a]	Corrosion Rate,[b] μm/yr	Remarks
AISI 1008	Cu_2S	>3000	Complete reaction in 500 hr.
	FeS	460[c]	Severe intergranular attack.
Type 304 SS	Cu_2S	5.3	Intergranular attack; Cu deposition.
	FeS	3.6	---
	CoS_2	>6400	Complete reaction in 500 hr.
	FeS_2	>6000	Complete reaction in 500 hr.
Nickel	Cu_2S	+9.0	Cu deposition.
	FeS	+10	Fe-Ni reaction layer.
	CoS_2	>6600	Complete reaction in 500 hr.
	FeS_2	>6600	Complete reaction in 500 hr.
Inconel 625	Cu_2S	+290	Cu deposition.
	FeS	2.7	---
	CoS_2	>5400	Complete reaction in 500 hr.
	FeS_2	1000	---
Hastelloy B	Cu_2S	+190	Cu deposition.
	FeS	2.5	---
	CoS_2	750	Intergranular attack.
	FeS_2	490	Intergranular attack.
Molybdenum	CoS_2	+2.8	Probable MoS_2 layer.
	FeS_2	+1.0	Probable MoS_2 layer.

[a]Equal volume mixtures of the sulfide with LiCl-KCl eutectic.

[b]Each corrosion rate is the average for two or more tests lasting more than 500 hr. Values preceded by "+" represent the average rate of formation for a reaction layer; those preceded by ">" represent the minimum corrosion rate based on initial sample weight.

[c]Average corrosion rate for Armco iron.

In the CoS_2 corrosion tests, Inconel 625, 304 stainless steel, and nickel samples were completely reacted after 500 hr. X-ray diffraction analysis of the reaction products indicated that the sulfidation attack on these samples is similar to that observed in other aggressive, sulfur-bearing environments such as FeS_2. Hastelloy B had an average corrosion rate 50% higher than that observed in FeS_2 tests, and showed localized areas of deep intergranular penetration. Molybdenum demonstrated excellent corrosion resistance, with small weight gains indicative of the presence of a thin, but adherent, molybdenum sulfide layer.

In comparing the Cu_2S with the FeS test results and the CoS_2 with the FeS_2 results, some conclusions can be made. In general, the corrosion resistance of a nickel-base material is roughly equivalent for both the Cu_2S

and FeS environments; however, iron and its alloys are corroded more rapidly by the Cu_2S. This suggests that under charge conditions the presence of Cu_2S in an FeS electrode accelerates the attack on iron-base current collectors. In the CoS_2 environment, the corrosion rates of metals, with the exception of molybdenum, tended to be significantly higher than in the FeS_2 environment. This finding places further restrictions on alternative materials to molybdenum for use as components in FeS_2 electrodes using CoS_2 as an additive.

5. Cell Wetting Studies
(J. G. Eberhart)

The internal resistance of a lithium/metal sulfide cell is determined in part by the extent to which the LiCl-KCl electrolyte fills the pores of the separator. Pore filling is related to the wettability of the separator material by the electrolyte. Thus, experiments are in progress to identify the factors which influence the wettability of the separator material (ANL-77-35, p. 43).

A pretreatment process has been developed for BN separators that greatly improves their wettability by LiCl-KCl electrolyte. This process involves the immersion of BN fabric in molten $LiAlCl_4$; after the excess $LiAlCl_4$ is drained, the BN fabric can be easily penetrated by LiCl-KCl electrolyte at 400°C. (Untreated BN fabric exhibits difficult-to-penetrate behavior.) Contact angle measurements have shown that LiCl-KCl will spread over a hot-pressed BN surface (zero contact angle) after $LiAlCl_4$ is melted onto this surface. If the excess $LiAlCl_4$ is removed from the BN surface and LiCl-KCl is then melted onto this surface, the LiCl-KCl spreads at temperatures above 350°C. This same electrolyte has an advancing contact angle of about 140°C (nonwetting) on an untreated BN surface.

Boron nitride surfaces are probably covered by a thin layer of boric oxide that reacts with the acidic $AlCl_4^-$ ion, possibly forming an oxychloride ion. The fluxing action of the $LiAlCl_4$ may expose the true BN surface, which is much more wettable than B_2O_3. This difference in wettability is related to the surface tensions of these solids, which are estimated to be about 0.1 J/m^2 for B_2O_3 and at least 0.8 J/m^2 for BN.

Molten LiCl-KCl penetration tests are also under way on some of the rigid, porous Y_2O_3 separators (see Section IV.A.3). The sintered foams and sintered powders that have been tested to date display easy-to-penetrate behavior. However, the powder specimens require longer times than the foam specimens for the initial salt penetration and for subsequent drainage through the porous specimen. A full report will be given on the porous Y_2O_3 separators when the testing is completed.

6. Cell Degassing
(J. G. Eberhart)

The degassing and attendant pressure build-up which can occur during the operation of a cell are probably detrimental to its efficiency and lifetime. Thus, a study was initiated to characterize, by mass spectrometry, the gaseous species produced while cells are in a charge, discharge, or open-circuit mode. A vacuum system required for these experiments was completed, and has been attached to a Varian quadrupole mass spectrometer. The pump is

operational, and when the vacuum gauge installation is complete the system will be given its final testing.

7. Electrical Conductivity Studies
(J. G. Eberhart)

The electrical resistance of a cell separator filled with electrolyte is an important part of the total cell resistance. Thus, a study of the electrical conductivity of two-phase (conducting and nonconducting), electrolyte-separator systems has been initiated. The initial effort of this study was an examination of the literature on ionic conductivity of molten LiCl-KCl eutectic and theories related to the conductivity of two-phase systems. The information already available on this subject permits reliable estimates to be made on the conductivity of electrolyte-separator systems related to the battery program.

8. Postoperative Cell Examinations
(F. C. Mrazek, N. C. Otto, J. E. Battles)

Postoperative examinations are conducted on test cells primarily to evaluate the performance of various construction materials and components--in particular feedthroughs, current collectors, electrode separators, and cell housings. These examinations provide important information, not only on the compatibility of cell components with the cell environment, but also on the performance and behavior of the lithium-aluminum and metal sulfide electrode materials. Table IV-3 presents the results of the 16 cell examinations that were performed during this period as well as some observations and conclusions as to the causes of cell failure.

The vertical, prismatic cells that have undergone postoperative examinations over the last 2 years (this quarter included) have been reviewed. A total of 49 FeS and FeS_2 cells were examined in this period. The operation of 36 of the 49 cells was terminated due to short circuits; operation of the remaining cells was terminated due to declining performance. The mechanisms of failure for all 49 cells are given in Table IV-4.

The primary causes of short circuits were as follows: (1) extrusion of active material from one electrode and subsequent contact with the opposing electrode, 16 cases; (2) copper deposition in the separator of cells with Cu_2S additives, 7 cases; and (3) penetration of the separator by the honeycomb current collector, 4 cases.

Declining performance generally indicates the presence of a partial short circuit across the separator. This behavior has been attributed to a buildup of a large quantity of metal and metal sulfide particles (through migration or deposition) within localized areas of the separator. The factors involved in this behavior include cell overcharge, polarity reversal, and defects in the separator/retainer; other factors, as yet undetermined, may also be involved. A total of 11 cells were classified in this category.

The presence of Li_2S in the separator of FeS_2 cells has not been shown to be a cause of the short circuits. However, this behavior is a contributing factor in declining cell capacity through the loss of lithium and

Table IV-3. Summary of Postoperative Examinations

Cell Number	Type of Cell	Limetime		Reason for Termination	Postoperative Examinations
		Days	Cycles		
EP-I-1-B-1	LiAl/FeS-Cu_2S	65	66	Declining performance	Near short caused by positive current collector honeycomb cutting through separator and approaching negative retaining screen. Copper was present in the separator near the positive electrode; however, the majority of the Y_2O_3 separator was free of active material and unreacted.
EP-2B5	LiAl/FeS_2-CoS_2	91	127	Declining performance	A 70% expansion of the negative electrode compressed the positive, thus driving the positive current collector honeycomb through the BN separator into contact with a retaining screen at negative potential.
M-2	LiAl/FeS_2-CoS_2	24	30	Short circuit	Low resistance areas were caused by the close proximity of a stainless steel gasket face around the negative electrode tray and the Hastelloy B picture frame on the positive electrode. The presence of metallic particles in the separator from corrosion of the Hastelloy B may also have contributed. Y_2O_3 felt was an effective particle retainer for the positive electrode but allowed minor intrusion of active material from the negative electrode. The Y_2O_3 separator appeared to have reacted in several areas.
EP-2A5	LiAl/FeS_2-CoS_2	129	315	Declining performance	Excessive expansion of the negative electrodes caused compaction of the positive electrode which in turn forced FeS particles into the BN separator. This expansion also caused the positive electrode honeycomb to cut the ZrO_2 and BN fabric.
EP-2A7	LiAl/FeS_2-CoS_2	19	61	Declining performance	Same as EP-2A5.
FM-1	LiAl-4 wt % In/FeS-Cu_2S	159	320	Declining performance	The In addition to the negative electrode resulted in larger, more rounded, particles of LiAl. Chemical analyses showed that the In remained within the negative electrode, with slightly more in the front half of the electrode than the back.
FM-3	LiAl-816 wt % Sn/FeS-Cu_2S	138	232	Declining performance	The Sn addition to the negative electrode resulted in a very fine particle size range for LiAl. Chemical analyses showed that the Sn remained within the negative electrode.
EP-2B6	LiAl/FeS_2-CoS_2	182	237	Accidentally overcharged	Resistance measurements indicated a short or near short throughout the cell. However, no evidence of a conductive path could be found microscopically. The separator contained more Li_2S and associated Fe than usual, apparently a result of the overcharge. The unusually large amount of iron in the separator was probably responsible for the short.
CA-10	Mg_2Si/CaS-Fe	47	125	Declining performance	Severe attack of the ZrO_2 cloth in both electrodes evident by a marked color change in the individual fibers and physical disintegration of the cloth. The presence of calcium seemed to be helpful in reducing corrosion because no evidence was found of Si or Mg reaction with the mild steel current collector in the negative electrode.

Table IV-3. (contd)

Cell Number	Type of Cell	Limetime		Reason for Termination	Postoperative Examinations
		Days	Cycles		
DK-52	$LiAl/TiS_2$	15	17	Short circuit	The short circuit believed to have been caused by a cycler malfunction which may have moved metallic lithium into the separator (althcugh no metallic particles could be observed). X-ray diffraction analyses revealed metallic Al in the negative electrode and $LiTiS_2$ in the positive, confirming a fully discharged condition.
G-02-002	$LiAl/FeS-Cu_2S$	52	43	Test completed	Restraining plates prevented a thickness change, but the edges and bottom bulged 6 mm beyond their original form. The X-MET current collectors in both negative electrodes were all in the back half of the electrode. Chemical analyses show that the $CaCl_2$ added to the negative electrode migrated into the separator and formed CaS.
PC-2-01	$LiAl/FeS-Cu_2S$	31	38	Short circuit	Some areas of the BN fabric separator showed larger than normal open channels between the strands of yarn. These interstices contained stringers of metal which apparently moved out from the negative electrode and are believed to be responsible for the multiple conductive paths through the separator.
TO-5	$LiAl/FeS_2-CoS_2$	22	25	Short circuit	The front two-thirds of the cast LiAl plaque had been changed to a sponge-like structure and the overall thickness doubled. A similar observation was made on cells TO-2 and TO-3. The BN felt separator appears to be functioning well as particle retainer.
CRC-4	$LiAl/FeS_2-CoS_2$	56	96	Failure to accept charge	Fabricated in air with cast negative electrodes. Excessive local swelling because of uneven loading caused the positive honeycomb current collector to cut through the separator and contact the negative retaining screen. No evidence the cast Li-Al structure remained in the negative electrode--probably a result of casting the electrode in a Retimet foam.
TK-12	$LiAl/FeS-Cu_2S$	37	50	Test completed	Carbon, powder-bonded positive electrode. The matrix of the positive electrode was X_{Cu} phase with evenly distributed carbon particles. Distributed through the matrix were areas of high carbon concentration with associated fine iron particles and minor FeS.
TK-15	$LiAl/FeS-Cu_2S$	35	50	Test completed	Graphite, powder-bonded positive electrode. The matrix of the positive electrode was FeS with evenly distributed graphite particles. There were also several very large and evenly distributed areas of X_{Cu} phase with a slightly lower graphite content. Some local concentrations of graphite were found associated with fine iron particles.

Table IV-4. Cell Failure Mechanisms

Cause of Cell Failure	FeS Cells		FeS_2 Cells		Cell Total	
	No.	%	No.	%	No.	%
Extrusion of material	6	32	10	33	16	33
Metal in separator	7	37	3	10	10	22
Metal sulfide in sep.	1	5	3	10	4	8
Test error	0	0	3	10	3	6
Assembly error	0	0	3	10	3	6
Cut separator	1	5	6	20	7	14
Broken lead	0	0	1	4	1	2
Unknown	4	21	0	0	4	8
Unexamined	0	0	1	4	1	2

sulfur. Interestingly, Cell YF-1, an FeS_2 cell with a Hastelloy B Foametal* current collector, showed essentially constant capacity throughout its lifetime. The amount of Li_2S in this cell's separator was negligible; however, the Hastelloy was completely reacted, thus reducing the sulfur that was active in the cell.

The following corrective actions to prevent cell failure have been recommended: (1) electrode frames adequate to prevent extrusion of the active material, (2) elimination of the Cu_2S additive to FeS cells, and (3) addition of protective screens over the honeycomb current collector.

B. Cell Chemistry
(M. F. Roche)

The objectives of the cell chemistry studies are (1) to investigate specific chemical and electrochemical problems that arise in the development of cells and batteries, (2) to conduct studies that are expected to lead to improvements in the electrodes and in cell design, and (3) to provide a basic understanding of the processes that occur within cells.

1. Cyclic Voltammetry of FeS_2
(S. K. Preto, M. F. Roche)

A serious problem with $LiAl/FeS_2$ cells is their high rate of capacity decline with cycling. Declines during early cycling of as much as 1% per cycle are not uncommon in sealed cells. Postoperative examinations have shown that Li_2S in conjunction with iron appears as a more or less continuous layer in the electrode separators. It is very likely that the capacity decline and separator blockage by Li_2S are directly related. The above observations prompted a decision to examine the kinetics of the FeS_2 electrode reaction in greater detail.

*A product of Foametal, Inc., Willoughby, Ohio.

The reactions in LiAl/LiCl-KCl/FeS_2 cells were studied previously through a combination of metallography, X-ray diffraction, and out-of-cell preparations (ANL-8057, p. 22). Starting from the discharged state, the known phase boundaries were:

(a) Li_2S + Fe (full discharge)

(b) Li_2FeS_2 (50% charge)

(c) $Li_4Fe_2S_5$ + FeS (about 67% charge)*

(d) FeS_2 (full charge)

An additional phase may occur between boundaries (c) and (d) according to the metallographic studies described in the next section.

Slow-scan voltammetry was employed to search for the source of the problems with FeS_2 electrodes. The FeS_2 reactions were studied in LiCl-KCl electrolyte at 405°C using LiAl (45 at. % Li) counter and reference electrodes. The FeS_2 working electrode (area, 5 cm^2) consisted of 92 mg of FeS_2 in graphite foam within a molybdenum housing. The voltage scan rate was 0.015 mV/sec over a range of 1 to 2 V *vs.* LiAl.†

A typical voltammogram for this electrode is shown in Fig. IV-1;‡ charge peaks are shown above the horizontal axis and discharge peaks are below. A qualitative interpretation of the peaks is given on the figure.

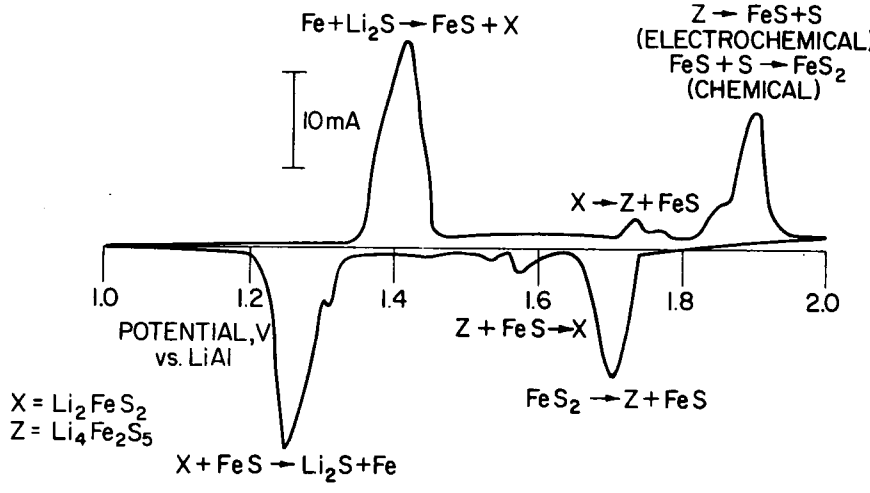

Fig. IV-1. Voltammogram for FeS_2 in LiCl-KCl Electrolyte at 405°C

*The composition of the $Li_4Fe_2S_5$ is known only approximately, and the FeS is probably slightly deficient in iron.

†All voltages in this section are versus a LiAl reference electrode.

‡Repeated sweeps reproduce this voltammogram.

The low-voltage peaks, in the range from 1.2 to 1.5 V, are complex. They consist of overlapping peaks for FeS (see ANL-77-35, p. 57) and for the half-discharged product of FeS_2, Li_2FeS_2. The presence of FeS and the discharge product of FeS_2 in this voltage range can be explained by the fact that the working electrode, although loaded with stoichiometric FeS_2, lost some sulfur during cycling and became a mixture of FeS and FeS_2. The electrochemical behavior of the electrode in this voltage range is acceptable; the charge and discharge meet at the same voltage, 1.35 V. This voltage is the measured emf of the lower voltage plateau in LiAl/FeS_2 cells (ANL-77-17, p. 46). Thus the reaction,

$$2Li_2S + Fe + 2Al \rightleftarrows Li_2FeS_2 + 2LiAl$$

exhibits satisfactory electrochemical reversibility.

Poor electrochemical reversibility is exhibited by the FeS_2 electrode in the higher voltage range, 1.5 to 2.0 V. The large voltage separation between the major charge and discharge in this voltage range indicates that the reaction path during charge differs from that during discharge. The major discharge peak begins at 1.74 V, which is the emf observed on the upper voltage plateau in LiAl/FeS_2 cells (ANL-77-17, p. 46). However, the major charge peak does not begin at 1.74 V but at 1.86 V; this voltage is close to the calculated emf for oxidation of Li_2S to sulfur, 1.87 V, as well as for oxidation of $Li_4Fe_2S_5$ to a mixture of FeS_2 and sulfur, 1.85 V (ANL-77-35, p. 50). Thus, the discharge of FeS_2 to a mixture of $Li_4Fe_2S_5$ and FeS is not kinetically hindered, whereas the electrochemical charge reaction is kinetically hindered.

In view of the complexity of the phases known to be present in the electrode and the possibility of others being present, it is not possible at this time to formulate the precise combination of electrochemical and chemical steps that lead ultimately to formation of FeS_2 at full charge. However, the preceding voltammetric results along with the metallographic findings give strong evidence that the charge reaction proceeds exclusively through electrochemical formation of a soluble, sulfur-rich species which is then transferred through the electrolyte to react chemically with FeS. The soluble species, which originates from phases with a high ratio of sulfur to transition metal such as $Li_4Fe_2S_5$, may contain both sulfur and iron. Another possible source of a soluble iron species, $FeCl_2$, can be detected in the voltammogram shown in Fig. IV-1. An upsweep in current, which is believed to result from oxidation of FeS to a mixture of $FeCl_2$ and FeS_2, underlies the 1.86-V charge peak.

It is possible that these soluble sulfur and iron species diffuse from the positive electrode and are reduced by Li as they approach or come into contact with the negative electrode. Thus, Li_2S associated with iron in the BN separator of FeS_2 cells appears to be a consequence of poor charge kinetics for FeS_2. Slow-scan voltammetry is now being used to search for additives that will promote rechargeability of FeS_2 at 1.74 V and thereby reduce the formation of soluble sulfur and iron species.

2. Phases in FeS_2 Electrodes
(A. E. Martin, Z. Tomczuk)

Phases present at various stages of discharge and charge of FeS_2 electrodes in Li-Al/LiCl-KCl/FeS_2 cells were studied previously through a combination of metallography, X-ray diffraction, and out-of-cell preparations (ANL-8057, p. 22). These earlier tests were conducted on cells that had been cycled repeatedly. Termination of cell operation during the first discharge or charge has yielded additional information. For example, metallographic examination of an FeS_2 electrode (1 A-hr capacity) after 31% of its first discharge in a Li-Al/LiCl-KCl/FeS_2 cell has revealed the presence of a new phase in the FeS_2 discharge path. Because of the relatively poor electronic conductivity of this electrode design (a graphite housing with no current collector added), all discharge zones were observed in this electrode. Proceeding from the back of the electrode, which was in contact with the graphite housing, the horizontally oriented zones were:

(1) Li_2S particles and fine iron particles,

(2) Li_2FeS_2 particles with a few J-phase ($LiK_6Fe_{24}S_{26}Cl$) particles,

(3) $Li_4Fe_2S_5$ particles and fine $Fe_{1-x}S$ particles,

(4) FeS_2 particles with an adhering layer of a new phase, and

(5) unreacted FeS_2 particles.

Attempts are now being made to determine the composition of the new phase (in zone 4) by heating Li_2FeS_2 and FeS_2 mixtures with electrolyte.

In order to examine charge reactions, an electrode containing Li_2FeS_2 (as -60 to +100 mesh particles) was assembled, and was charged in a Li/LiCl-KCl/Li_2FeS_2 cell. The charge was stopped at a point corresponding to 50% removal of lithium from Li_2FeS_2. The phases found by metallographic examination of this electrode were Li_2FeS_2, the new phase, $Li_4Fe_2S_5$, and $Fe_{1-x}S$ particles having a surrounding layer of FeS_2. No instances of FeS_2 formation directly from $Li_4Fe_2S_5$ or from the new phase were detected. Several of the Li_2FeS_2 electrodes were started with an equimolar mixture of FeS and Li_2FeS_2. Partial charging of these electrodes led to FeS_2 formation on the surfaces of the added FeS particles, as well as on the surfaces of $Fe_{1-x}S$ particles generated by oxidation of Li_2FeS_2. These results indicate that the charge mechanism involves transfer of sulfur, via a soluble species, from both $Li_4Fe_2S_5$ and the new phase to FeS particles.

The new phase is an important factor in the problem of achieving electrochemical reversibility in FeS_2 electrodes because it surrounds FeS_2 particles during discharge but does not convert directly to FeS_2 during charge. Therefore, the properties of this new phase will be examined in greater detail.

3. Titanium Disulfide Electrode Development
(K. E. Anderson, D. R. Vissers)

Titanium disulfide is being evaluated as a possible substitute for FeS_2 electrodes in cells with negative electrodes of LiAl and with an electrolyte of LiCl-KCl molten salt. The relatively small amount of swelling, about 30%, that occurs when TiS_2 is discharged to $LiTiS_2$ also makes this electrode a candidate for use in molten-salt cells having liquid-lithium electrodes. The disadvantage of a relatively low theoretical capacity for TiS_2 (0.24 A-hr/g TiS_2 *vs.* 0.45 A-hr/g FeS_2 if discharged to Li_2FeS_2) is offset by its ability to operate with a very small volume fraction of electrolyte (approximately 15%) and by its good electrochemical reversibility (ANL-77-17, p. 46).

Titanium disulfide was obtained from three vendors who stated that their products were at least 99.9% pure. Preliminary electrochemical and chemical tests showed that only one of these products had adequate purity and electrochemical activity for a preliminary evaluation of the TiS_2 electrode. X-ray diffraction analyses* of this material indicated a trace of TiO_2 in the TiS_2. Chemical analyses† gave 41.9 wt % titanium and 56.6 wt % sulfur, or a purity of 98.5%.

Three electrodes (surface area, 11.4 cm^2) with capacities from ∿1 to 4 A-hr were pressed to about 70% of theoretical capacity density from the above material. These electrodes contained 5.5 g (0.20 cm thick), 11 g (0.40 cm thick), and 16.5 g (0.66 cm thick) of TiS_2, and they were cycled repeatedly *vs.* 10 A-hr LiAl electrodes in LiCl-KCl electrolyte at 427°C using 2.25 V charge- and 1.0 V discharge-cutoff voltages (IR-included). Capacity density data for these three electrodes are given in Table IV-5. These data show that good utilization can be achieved at high current densities (70 mA/cm^2 charge, 140 mA/cm^2 discharge) even for the thick electrode.

Table IV-5. Performance of TiS_2 Electrodes

Electrode Thickness, cm	Theoretical Capacity Density, mA-hr/cm^2	Current Density, mA/cm^2		Utilization, %
		Charge	Discharge	
0.20	106	35	35	86
		70	140	75
0.40	210	35	35	85
		70	140	67
0.66	314	35	35	80
		70	140	70

*B. S. Tani, Analytical Chemistry Laboratory, ANL.

†W. E. Streets, Analytical Chemistry Laboratory, ANL.

A sealed, 75 A-hr (theoretical) $LiAl/TiS_2$ cell was fabricated by Eagle-Picher using their thin-electrode $LiAl/FeS_2$ cell hardware (ANL-77-17, p. 19). This cell developed a serious short circuit during its sixteenth cycle, but, prior to failure, it achieved specific energies of 67 and 46 W-hr/kg at the 10- and 4-hr rates, respectively. Efforts are now being made to obtain TiS_2 of very high purity in order to better evaluate the cycle life and specific energy of $LiAl/TiS_2$ cells.

C. Advanced Battery Research
(M. F. Roche)

The objective of this work is to develop new secondary cells that use inexpensive, abundant materials. The experimental work ranges from cyclic voltammetry studies and preliminary cell tests through the construction and operation of engineering-scale cells for the most promising systems. The studies at present are focused on the development of new cells with molten-salt electrolytes. During this quarter, most of the studies consisted of cycling tests of small-scale, alkaline-earth/metal-sulfide cells.

1. Positive Electrodes for Calcium Cells
(L. E. Ross, J. D. Arntzen, K. E. Anderson, D. R. Vissers, S. M. Faist*)

Earlier studies of calcium systems in $LiCl-KCl-CaCl_2$ electrolyte dealt mainly with development of a negative-electrode alloy having acceptable polarization characteristics (ANL-77-17, p. 52 and ANL-77-35, p. 53). These studies culminated in the development of a Ca-Mg-Si negative electrode that approached the performance of the lithium electrode, LiAl. Tests of new positive electrodes have been emphasized in recent studies.

In ANL-77-35, p. 57, oxidation of iron to $FeCl_2$ was found to occur in calcium cells with FeS positive electrodes; subsequent iron deposition on the negative electrode led to short-circuiting. Calculated emfs of binary transition-metal sulfides (ANL-77-17, p. 50) indicate that titanium disulfide and nickel sulfides avoid the formation of metal chloride solutions and produce high specific energies. In this period, these sulfides were tested in small (capacity, 1 to 5 A-hr) calcium cells.

The TiS_2 positive electrode was evaluated in a $CaAl_2$ (9 A-hr)/TiS_2 (7.5 A-hr) cell at 450°C. The electrolyte in this cell consisted of LiCl (55 mol %) -KCl (37 mol %) -$CaCl_2$ (8 mol %). The positive electrode was a 0.6-cm-thick and 2.5-cm-dia pressed disc held in a molybdenum housing; a porous iron structure within an iron housing contained the $CaAl_2$ powder. This cell was operated for 26 cycles at current densities of 13 to 150 mA/cm^2. The coulombic efficiency averaged 90%, and the TiS_2 electrode utilization varied from 82% at 13 mA/cm^2 to 40% at 150 mA/cm^2. However, X-ray diffraction analysis† showed that the product of TiS_2 discharge in the $LiCl-KCl-CaCl_2$ electrolyte was $LiTiS_2$ rather than a calcium compound. Therefore, because large composition shifts in the electrolyte create salt crystallization problems, this cell is a poor candidate for further development.

---

*Resident Student Associate, Massachusetts Inst. of Tech.

†B. S. Tani, Analytical Chemistry Laboratory, ANL.

Two $CaAl_2/NiS$ cells (same electrolyte as for the $CaAl_2/TiS_2$ cell above) with positive electrode capacities of 1 and 5 A-hr were tested. The NiS was contained in a porous graphite matrix within a graphite housing. The negative electrodes had capacities about four times those of the positive electrodes, and were prepared as described above for the $CaAl_2/TiS_2$ cell. These cells, which were operated for about 30 cycles, achieved positive-electrode utilizations of about 80% at 20 mA/cm^2 and coulombic efficiencies of more than 95%. It was concluded that this electrode is a good candidate for continued development even though the amount of nickel must be kept to a minimum owing to low availability and high cost. Nickel sulfide electrodes are being examined in larger cells, and the properties of NiS_2 are being studied in small cells.

In calcium cells, iron oxidation leading to $FeCl_2$ in solution competes with the reaction of iron and calcium sulfide to form FeS (ANL-77-35, p. 59). This problem is aggravated when excess iron is added as a current collector to the positive-electrode mix. Carbon current collectors were tested in iron sulfide electrodes to study their ability to control the iron oxidation problem. Of two carbons tested, acetylene black and chopped graphite fibers, only the chopped graphite fibers were readily wet by mixtures of LiCl-KCl-$CaCl_2$ molten salt and CaS. Tests were then conducted on two, 5 A-hr positive electrodes (3.7-cm dia.) that were prepared in graphite housings. These electrodes contained 15 wt % chopped graphite fibers, were prepared uncharged using mixtures of iron and CaS, and were operated in positive-electrode-limited cells *vs.* a $Ca_x(Mg_2Si)$ electrode. Neither cell gave acceptable performance. Maximum sulfur utilizations were about 50%, and the coulombic efficiencies declined to below 75% by the thirtieth cycle. Therefore, carbon does not appear to solve the problems (namely, poor capacity and coulombic efficiency) of iron sulfide electrodes in calcium cells.

Chalcopyrite was tested in a $CaAl_2/CuFeS_2$ (graphite) cell in which the cell capacity was limited by the positive electrode (1 A-hr). A utilization of 75% was obtained at 20 mA/cm^2. However, chalcopyrite is expected to have the same oxidation problem (namely, formation of metal chloride in solutions) as has been observed in Ca/FeS cells. Consequently, this electrode does not appear to be a good candidate for scale-up studies.

Some ternary sulfides, such as Fe-Ti-S compounds, may have satisfactory utilization and resistance to metal chloride formation. Tests of these more complex sulfides are planned. At present, the only acceptable sulfide electrode for calcium cells is nickel sulfide; this electrode will be tested in a compact, 75 A-hr $Mg_2Si/Ni(CaS)$ cell to determine whether calcium cells can be operated with high coulombic efficiency and electrode utilization.

2. Magnesium Cell Development
(Z. Tomczuk)

Prior tests of $Mg/NaCl-KCl-MgCl_2/FeS_2$ cells demonstrated that these 1.53-V cells had good electrochemical reversibility (ANL-76-35, p. 53), but poor cycle life. The major problem was short circuits caused by the formation of dendritic magnesium deposits on the negative electrode. Modified magnesium electrodes have been tested as alternatives to pure magnesium in a search for solutions to the dendrite problem. Potential negative electrode systems include: (1) magnesium with a dissolved "leveling" additive that will cause

formation of smoother electrodeposits; (2) magnesium intermetallics, such as Mg_2Al_3, that are solids at cell operating temperatures; and (3) liquid magnesium alloys such as magnesium solutions in zinc. Each of these possibilities is being examined in small-scale cell tests. In addition, other system variables (salt composition, positive electrode, and separator material) are being studied.

A cell, Mg_2Al_3 (8 A-hr)/KCl-NaCl-$MgCl_2$/FeS_2 (1 A-hr), was operated for three weeks at current densities of 8 to 18 mA/cm^2. The emf was 1.49 V at 430°C, the upper-plateau utilization of the FeS_2 was 90% at 8 mA/cm^2, and the coulombic efficiency was 97%. The operating characteristics of this system will be studied in more detail in larger scale cells; in addition, some cells employing the Mg_2Al_3/FeS_2 couple will be operated at 375°C in LiCl-KCl-$MgCl_2$. A Mg-Zn/NaCl-KCl-$MgCl_2$/FeS_2 cell in which the capacity was limited by the positive electrode was operated for two weeks (20 cycles) with high coulombic efficiency (greater than 90%) and a positive-electrode utilization of 60%. The positive electrode had a theoretical capacity of 1 A-hr; the negative electrode, an equimolar mixture of Mg and Zn, was a liquid at the cell operating temperature, 450°C. These tests demonstrated that the Mg/FeS_2 couple can be cycled successfully with acceptable coulombic efficiency. Scale-up studies have therefore been initiated.

V. Li-Si/FeS CELL AND BATTERY DEVELOPMENT--ATOMICS INTERNATIONAL

Positive electrode development has focused on material optimization of the electrode structure. Small compact cells were operated in this period with FeS and Li_4Si electrodes. Research efforts continued toward achieving theoretical coulombic efficiencies with cells charged to the +48 mV (*vs.* Li) plateau. Charging to lower cell potentials resulted in high coulombic efficiencies. Occasional delamination of the nickel current collector plate from the back side of the honeycomb structure in the positive electrode has been observed with some of the cells in which high active material utilization loading was used; however, no rupture of the porous nickel particle retainer was observed. Modifications to the bonding process are under way to minimize any potential bonding weaknesses.

Both electrode coatings and additives to the negative active material are showing promise of significantly reducing corrosion at the negative electrode. Extended corrosion tests are presently under way to gain more insight into the relative merits of each of these approaches.

Progress has been made toward optimization of powder separators in compact cells. Candidate powders so far investigated have been AlN and Si_3N_4. Some preliminary screening tests have been completed using CaO powder which shows promise as a candidate material. A cell using Si_3N_4 powder as the separator performed with coulombic efficiencies of 100%; this test was terminated owing to a faulty braze joint at the positive electrode.

Preliminary testing of honeycomb Si_3N_4 separators in compact cells has shown consistently high coulombic efficiencies and utilizations. Silicon nitride honeycomb (1-mm thick) has been fabricated, and is planned for evaluation in intermediate-size cells.

Testing of the 1 kW-hr instrumented thermal cell continues through 100 cycles and a wide variety of cycling regimens. Excellent reproducibility of thermal data has been achieved, and these data are undergoing analysis.

The 150 W-hr demonstration cell has completed 1,330 cycles of operation. The procurement of materials for the 2.5 kW-hr load-leveling cell has been completed.

REFERENCES

1. *United States Transit Industry Market Forecast*, American Public Transit Association (1976).

2. Booz-Allen Applied Research, *Transbus Operational, Passenger, and Cost Impacts*, p. 53 (1976).

3. L. J. Lawson, *Study of Flywheel Energy Storage*, prepared for Urban Mass Transportation Administration (1976).

4. A. Zuckerberg, Transportation Systems Center, Cambridge, Mass., personal communication (1976).

5. P. J. Martin, *Stored Energy Road Vehicles*, Stanford Research Institute (1976).

APPENDIX A

STATISTICAL DATA ON CELL PERFORMANCE

Figure A-1 depicts the number of cycles achieved by fifty-seven experimental and industrial cells that were operated during the past year (some of these cells are still in operation). The cycle life data of Fig. A-2 were derived from the data in Fig. A-1. The mean cycle life is 165 cycles for the FeS cells and 196 for the FeS_2 cells. However, these values have very large standard deviations that result from the numerous cell designs tested.

Table A-1 shows the highest performance and lifetime achieved by the FeS and FeS_2 cells that were operated in April-June 1977.

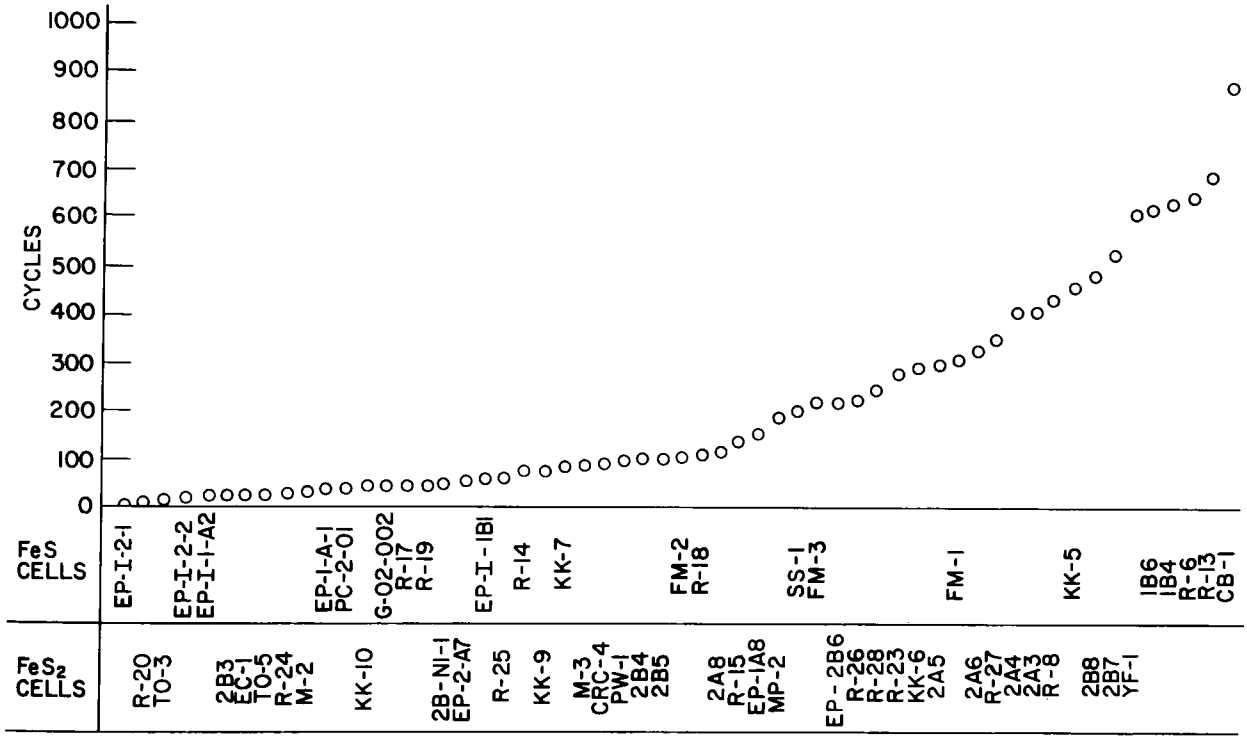

Fig. A-1. Cycle Life Data of FeS and FeS_2 Cells

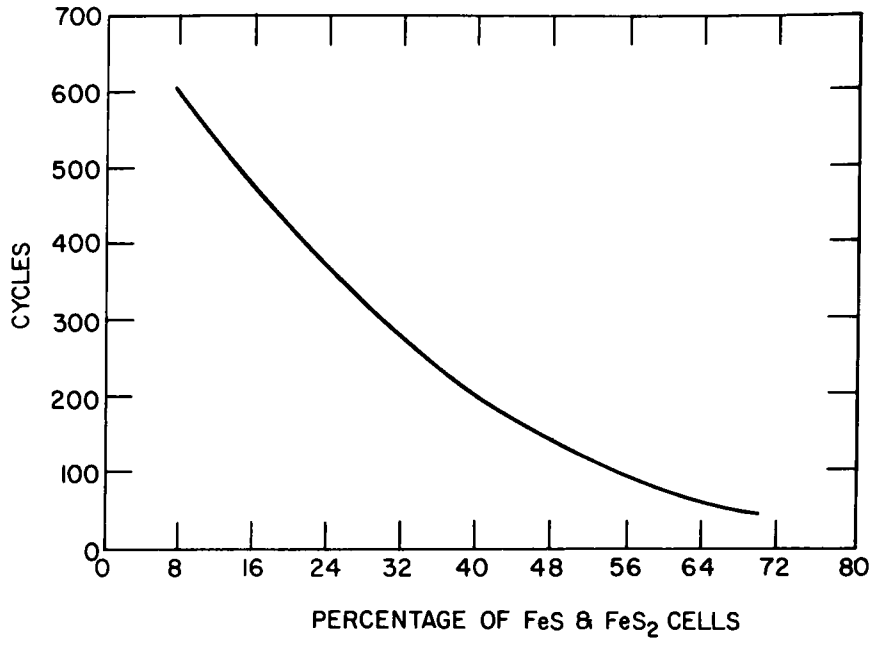

Fig. A-2. Number of Cycles *vs.* Percentage of Cells

Table A-1. Highest Cell Performance for April-June 1977

Cell Type	Specific Energy, W-hr/kg	Specific Power, W/kg	Cycles
FeS Cells			
I-3-C-1	72 (10 hr)[a]	-	-
1B4	60 (10 hr)	-	>581
CB-1	-	-	>945
FeS_2 Cells			
I-6-A-1	72 (4 hr)	-	-
2A5	-	68	-
2B7	65 (4 hr)	-	400
M-2	115 (5 hr)	167	-

[a]Numbers in parentheses indicate discharge rate.

[b]The ">" symbol indicates that operation is continuing.

APPENDIX B.

SUMMARY OF CELL TESTS

Appendix B. Summary of Cell Tests

Cell Description[a]	Max. Performance @ Indicated Rate[b] A-hr	W-hr	Rates, hr Disch.	Charge	Initial Eff.,[c] % A-hr	W-hr	Life Characteristics Days[d]	Cycles[d]	% Decline in[e] Capacity	Energy	A-hr Eff.	W-hr Eff.	Remarks
1A6, Li-Al/FeS-Cu_2S, C, S, 78/78, 13.5 × 15.6 × 2.3 cm, 1.35 kg	55	69	8	8	99	83	66	96	0	0	0	0	Operated to obtain performance characteristics of EP thin cells. Terminated to make room for next test.
2A7, Li-Al/FeS_2-CoS_2, C, S, 78/78, ~13.5 × 15.6 × 2.3 cm, 1.35 kg	57	77	4	5	99	85	20	64	37	24	38	50	Test of charging methods using EP thin cells. Constant power discharge. Computer controlled, current-limited and constant-voltage charge. Cell terminated.
2A8, Li-Al/FeS-CoS_2, C, S, 78/78, 13.5 × 15.6 × 2.3 cm, 1.32 kg	57	77	4	5	99	85	78	136	35	33	0	0	Test of charging methods using EP thin cells. Constant power discharge. Current-limited (15 amp), constant-voltage charge. Cell terminated.
2B8, Li-Al/FeS_2-CoS_2, C, S, 149/149, 13.5 × 15.6 × 3.8 cm, 1.990 kg	118 117	159 157	11.8 9.0	11.8 9.0	99	82	>314	>488	56	61	7	18	Start-up and operation with cell blanketed in Kaowool insulation, exposed to air.
I-3-B-1, Li-Al/FeS-Cu_2S, C, S, 170/127, 13.5 × 15.6 × 3.8 cm, 2.035 kg	101 88 76	131 108 92	10 5.9 3.8	10 5.9 3.8	99	81.5	>144	>238	6	5	4	4	Test of EP baseline cell, with slightly thinner positive and slightly denser negative. 67 W-hr/kg at 10-hr rate.
I-3-B-2, Li-Al/FeS-Cu_2S, C, S, 170/127, 13.5 × 15.6 × 3.8 cm, 2.02 kg	107	135	10	10	99	82	42	48	1.8	2.2	0	0	Test of EP baseline cell, with slightly thinner positive and slightly denser negative. 67 W-hr/kg at 10-hr rate. Cell terminated to make room for next test.
I-3-C-1, LiAl/FeS-Cu_2S, C, S, 193/145, 13.5 × 15.6 × 3.8 cm (shimmed cell), 1.72 kg	115	136	11	16	99	82	52	51	12	12	0	0	More compact EP cell, 4.2 mm thick positive electrode. 72 W-hr/kg and 56 W-hr/kg at 10- and 5-hr rates respectively. Cell terminated to make room for next test.
I-3-C-2, Li-Al/FeS-Cu_2S, C, S, 193/145, 13.5 × 15.6 × 3.8 cm (shimmed cell), 1.79 K	97	122	10	10	98	84	>41	>63	0	0	0	0	More compact EP cell, 4.2 mm thick positive electrode. 63 W-hr/kg at 10 hr rate. Constant current charge compared to constant voltage charge.
PC-2-01, Li-Al/FeS-Cu_2S-C, C, O, 150/140, 13.5 × 15.6 × 3.8 cm, 1.98 kg	98	122	10	10	95	82	31	38	16	15	15	12	Test of pellet cell concept for making large electrodes. 8.3 wt % carbon powder pressed in positive pellets. Terminated.

Cell Description[a]	Max. Performance @ Indicated Rate[b]		Rates, hr		Initial Eff.,[c] %		Life Characteristics						Remarks
									% Decline in[e]				
	A-hr	W-hr	Disch.	Charge	A-hr	W-hr	Days[d]	Cycles[d]	Capacity	Energy	A-hr Eff.	W-hr Eff.	
PNC-1-01, Li-Al/FeS-Cu_2S, C, O, 145/165, 13.5 × 15.6 × 3.8 cm, 2.13 kg	114	145	11	11	93	78	41	41	6	7	5	5	Test of pellet negative electrode. Terminated to make room for next test.
PFC-1-01, Li-Al/FeS_2-CoS_2, C, O, 150/133, 13.5 × 15.6 × 3.8 cm, 2 kg	101	138	10	10	98	77	>21	>19	8	7	3	3	First pellet cell with FeS_2 positive-difficulties welding heavy bus onto positive grid.
2B-Ni-1, Li-Al/FeS_2-CoS_2, C, S, 150/150, 13.5 × 15.6 × 3.8 cm, 2.05 kg	110	146	8.5	8.5	99	76	34	48	22	25	30	20	Baseline EP thick cell with Ni added to face of positive electrode. Terminated, poor coulombic Eff.
2B-Fe-1, Li-Al/FeS_2-CoS_2, C, S, 150/150, 13.5 × 15.6 × 3.8 cm, 1.88 kg	115	158	11	11	99	81	>14	>15	0	0	0	0	Baseline EP thick cell with Fe added to face of positive electrode.
I-4-1, Li-Al/FeS_2-CoS_2, C, S, 171/156, 13.5 × 15.6 × 3.8 cm, 2.18 kg	108	151	11	11	99	81	>28	>28	11	11	1	2	Baseline EP thick cell with offset positive terminal rod.
I-6-A-1, Li-Al/FeS_2-CoS_2, C, S, 199/156, 13.5 × 15.6 × 3.2 cm, 1.65 kg	97	133	10	10	99	82	>28	>37	2	1	0	1	More compact EP cell, with thinner and less porous electrode (positive). 72 W-hr/kg at 4-hr rate, peak power 57 W/kg
R-26, Li-Al/FeS_2-CoS_2, U, O, 103/127, 12.7 × 12.7 × 3.0 cm, 1.6 kg	87	122	5	6	100	75	90	240	50	50	45	50	Upper-plateau cell, assembled uncharged. Pressed Al wire, partially charged; negative; hot-pressed positive. Terminated.
R-27, Li-Al/FeS_2-CoS_2, U, O, 85/155, 12.7 × 12.7 × 2.7 cm, 1.3 kg	79	111	5	8	99	65	86	370	50	50	45	50	Upper-plateau cell, assembled uncharged. Negative electrode, pressed Al wire, partially charged with Li foil. Hot-pressed positive. Terminated.
R-28, Li-Al/FeS_2-CoS_2, U, O, 170/300, 12.7 × 12.7 × 5.1 cm, 1.9 kg	144	222	14	17	100	68	90	270	50	50	50	50	Upper-plateau cell, assembled uncharged. Negative electrode, pressed Al wire, partially charged with Li foil; positive electrode, hot-pressed, contains acetylene black. Terminated.

Appendix B. (contd)

Cell Description[a]	Max. Performance @ Indicated Rate[b] A-hr	W-hr	Rates, hr Disch.	Charge	Eff.,[c] % A-hr	W-hr	Life Characteristics Days[d]	Cycles[d]	% Decline in[e] Capacity	Energy	A-hr Eff.	W-hr Eff.	Remarks
R-29, Li-Al/FeS_2-CoS_2, U, S, 125/137, 12.7 × 12.7 × 3.5 cm, 1.90 kg	79 70 63	123 90 72	10 4 2	10 7 7	99	73	>50	>100	0	0	0	0	Upper-plateau cell, assembled uncharged. Negative electrode, pressed Al wire, partially charged with Li-Al plaque; hot-pressed positive.
VB-3, Li-Al/FeS_2, U, S, 146/118, 12.7 × 12.7 × 3.2 cm, 1.85 kg	65	97	6	12	97	76	>10	>10	0	0	0	0	Upper-plateau uncharged cell, completely assembled in air. Negative electrode, pressed Al wire, partially charged with Li-Al plaque. Hot-pressed X-phase positive.
CB-1, Li-Al/$CuFeS_2$, C, O, 148/147, 8.3 × 15.9 × 4.4 cm	67	72	5	5	98	67	>503	>890	30	28	3	0	Carbon-bonded positive; hot-pressed negative. 13 mΩ resistance.
SS-1, Li-Al/FeS-Cu_2S, C, S, 720/650, 25 × 35.6 × 3.8 cm, 11.5 kg	432	570	11	11	100	85	188	203	48	49	12	13	Carbon-bonded positive: iron Retimet negative. 3 mΩ resistance. Temporarily terminated.
FM-0, Li-Al/FeS-Cu_2S, C, S, 85/70, 13.0 × 15.2 × 2.5 cm, 1.67 kg	52	65	6	6	99	85	>62	>120	0	0	0	0	Eagle-Picher cold-pressed positive; iron Retimet negative Li-Al. Baseline cell. Slow break-in, 6.5 mΩ resistance.
FM-3, Li-Al-Sn/FeS-Cu_2S, C, S, 86/70, 13.0 × 15.2 × 2.5 cm, 1.65 kg	57	71	7	7	99	85	138	232	14	16	19	19	Eagle-Picher cold-pressed positive; iron Retimet negative Li-Al-8 wt % Sn alloy. Rapid break-in, 7.3 mΩ resistance. Terminated.
M-2, Li-Al/FeS_2-CoS_2, C, S, 201/146, 13.3 × 13.3 × 3.3 cm, 1.80 kg	141 136	190 213	5 11	12 12	95	68	24	31	11	10	37	0	Hot-pressed FeS_2-CoS_2 positive; hot-pressed Li-Al negative. Alloy is 55 at. % Li. Welded Mo terminal current collector connection. 3.2-4.8 mΩ resistance. Modified housing increased specific energy by 13% at 5-hr rate. Heat-treated Hastelloy B frame in positive Y_2O_3-felt separator/retainer. Terminated.

Cell Description[a]	Max. Performance @ Indicated Rate[b] A-hr	W-hr	Rates, hr Disch.	Charge	Eff.,[c] % A-hr	W-hr	Life Characteristics Days[d]	Cycles[d]	% Decline in[e] Capacity	Energy	A-hr Eff.	W-hr Eff.	Remarks
M-3, Li-Al/FeS_2-CoS_2, C, S, 103/74, 13.3 × 13.6 × 2.4 cm, 1.35 kg	60 73 71	82 110 112	2 5 10	8.5 10 8	98	78	>57	>90	25	31	28	33	Hot-pressed FeS_2-CoS_2 positive; hot-pressed Li-Al negative. Alloy is 55 at. % Li. Welded Mo terminal current collector connection. 4.2-5.5 mΩ resistance. Specific energy at 2-hr and 5-hr rate is same (83 W-hr/kg). Hastelloy B on positive replaced by Mo.
KK-5, Li-Al/FeS-$CuFeS_2$, U, S, 180/120, 5 in. × 5 in., 1.9 kg	93	107	5	10	99	85	336	465	15	14	0	0	Carbon-bonded Li_2S + Fe + Cu and Al wire plaque + Li-Al hot-pressed; >45 W-hr/kg at 2-hr rate. First sealed cell to reach 400 deep cycle goal of <10% capacity decline. 99.5% A-hr efficiency. 4.5 mΩ resistance. Terminated voluntarily.
KK-9, Li-Al/FeS_2-CoS_2, C, S, 150/140, 13.5 × 15.6 × 3.8 cm, 1.85 kg	110	151	10	10	>98	78	71	80	50	50	30	30	Carbon-bonded FeS_2-CoS_2 and cold-pressed LiAl electrodes. An EP cell with carbon-bonded positive. Performance has paralleled EP cells. Cell terminated after furance mulfunction to 550°C, shorting.
KK-10, Li-Al/FeS_2-CoS_2, U, S, 180/120, 13.5 × 15.6 × 3.8 cm, 2.2 kg	62	91	.4	5	90	70	25	40	0	0	0	0	Carbon-bonded X phase ($Li_2S \cdot FeS$); Al wire plaque + LiAl hot-pressed (EP). Cell fabricated in "air" with Al encapsulated LiAl plaques. Y_2O_3-felt particle retainer. Terminated due to decomposition of the experimental BN fabric.
KK-11, Li-Al/FeS_2-CoS_2, C, S, 100/75, 13.3 × 13.6 × 2.4 cm, 1.4 kg	71	105	5	7	98	83	>50	>90	8	10	3	4	Carbon-bonded FeS_2-CoS_2 and 55 at. % LiAl hot pressed electrodes. Welded Mo current collector, 3.5 mΩ cell resistance. Y_2O_3 felt separator/retainer. 75 W-hr/kg at 5 hour rates. 180 W/kg extrapolated power density.

Appendix B. (contd)

Cell Description[a]	Max. Performance @ Indicated Rate[b] A-hr	W-hr	Rates, hr Disch.	Charge	Eff.,[c] % A-hr	W-hr	Life Characteristics Days[d]	Cycles[d]	% Decline in[e] Capacity	Energy	A-hr Eff.	W-hr Eff.	Remarks
PW-1, Li-Al/FeS_2-CoS_2, C, S, 171/120, 12.4 × 14.0 × 2.8 cm, 1.55 kg	71 48	113 69	14 3	14 7	∿99	90	57	116	0	15.5	0	5	Y_2O_3-powder separator test. Hot-pressed FeS_2-CoS_2 (10 wt. %) positive; hot-pressed LiAl negative. Alloy is 50 at. % Li. Welded 5 mil perforated Mo sheet-terminal current collector. No negative current collector. Upper plateau, 10 mΩ IR. Terminated.
PW-2, Li-Al/Li_2S-FeS-CoS, U, S, 180/112, 12.4 × 13.0 × 2.8 cm, 1.43 kg	92 65	148 100	18.5 6	18.5 12	∿99	73.8	>25	>35	20	21	0	0	Y_2O_3-powder separator test. Hot-pressed Li_2S-FeS-CoS (10 wt. %) positive; hot-pressed Li-Al negative. LiAl alloy is 50 at. % Li. Welded Mo sheet-terminal current collector. Fe honeycomb in negative for current collection. Powder separator + electrolyte premixed at electrolyte melting temperature. Totally sealed cell. Upper plateau, 6-10 mΩ IR.
PW-3, Li-Al/Li_2S-FeS-CoS, U, S, 180/120, 12.4 × 13.0 × 2.8 cm, 1.35 kg	56	86	11	11	∿99	80	>6	>11	0	0	0	0	MgO-powder separator test. Hot-pressed Li_2S-FeS-CoS (10 wt. %) positive; hot-pressed Li-Al-LiAl negative. Fe honeycomb current collector in negative electrode. Powder separator + electrolyte premixed at melting temperature of electrolyte. Totally sealed cell, upper plateau.
A-4, Li-Al/FeS_2-CoS_2, U, O, 115/110, 11.7 × 12.7 × 3.5 cm, 1.2 kg	72	111	9	13	100	80	>54	>83	17	24	8	15	Upper-plateau cell, assembled uncharged. Welded Mo sheet current collector; Hastelloy B frame in positive. 12-13 mΩ resistance. Specific energy of 97 W-hr/kg at 9 hr rate and 102 W-hr/kg at 13-hr rate. New design.

[a]The letters U, C, O and S are used to indicate uncharged, charged, open, and sealed cells, respectively. The theoretical capacity is given for the limiting electrode. The capacity ratio is the ratio of the negative electrode capacity to the positive electrode capacity.

[b]Based on at least five cycles.

[c]Based on at least 10 cycles at the 5-hr discharge.

[d]The "greater than" symbols denote continuing operation.

[e]Percent decline from the maximum values at the 5-hr discharge, except where noted.

APPENDIX C.

SUMMARY OF BATTERY TESTS

Appendix C. Summary of Battery Tests

Battery Description[a]	Max. Performance @ Indicated Rate[b] A-hr	W-hr	Rates, hr Disch.	Charge	Eff.,[c] % A-hr	W-hr	Life Characteristics Days[d]	Cycles[d]	% Decline in[e] Capacity	Energy	A-hr Eff.	W-hr Eff.	Remarks
B7-S, Li-Al/FeS-Cu_2S, C, S. 149/149, 13.5 × 15.6 × 3.8 cm, 3.99 kg	100 77 57 35	246 176 124 78	10 5 3 1	9 6 4 4	99	74	>386	>595	47	22	11	11	Two Eagle-Picher thick electrode cells in series. Total life of 1B4 is 435 days, 629 cycles; 1B6, 408 days, 622 cycles. Now being operated with charge plus 4-hr equalization.
B10-S, Li-Al/FeS_2-CoS_2, C, S, 156/143, 13.5 × 15.6 × 3.8 cm, 12.41 kg	113 97	974 799	11 7	11 10	99	79	36	32	17	17	0	0	Six Eagle-Picher thick electrode cells (I-5-1, 3, 4, 5, 7, 8) in series. Started-up and conditioned. Two-hour equalization. Tested in case. Terminated, Cell I-5-1 developed leak.
B11-S, Li-Al/FeS_2-CoS_2, C, S, 156/143, 13.5 × 15.6 × 3.8 cm, 12.37 kg	78	686	10	10	99	86	52	67	12	12	0	0	Six Eagle-Picher thick electrode cells (I-5-2, 3, 4, 5, 7, 8) in series. Start-up of new cell inter-mixed with used cells. Bulk charge only. Terminated I-5-2 developed Leak.
B12-S, Li-Al/FeS_2-CoS_2 C, S, 156/143, 13.5 × 15.6 × 3.8 cm, 10.34 kg	81	606	10	10	99	∿86	>23	>34	64	67	2	4	Five Eagle-Picher thick electrode cells (I-5-3, 4, 5, 7, 8) in series. Equalization charge used.

[a]The letters U, C, O and S are used to indicate uncharged, charged, open, and sealed cells, respectively. The capacity ratio is the number of ampere-hours in the negative electrode over the number of ampere-hours in the positive electrode. In some cases, only the capacity of the limiting electrode is given.

[b]Based on at least five cycles.

[c]Based on at least 10 cycles at the 5-hr discharge.

[d]The "greater than" symbols denote continuing operation.

[e]Percent decline from the maximum values at the 5-hr discharge, except where noted.

Distribution of ANL-77-68

Internal:

M. V. Nevitt
R. V. Laney
P. R. Fields
S. A. Davis
B. R. T. Frost
G. T. Garvey
D. C. Price
K. E. Anderson
J. D. Arntzen
J. Barghusen
L. Bartholme
J. E. Battles
E. C. Berrill
W. Borger
C. A. Boquist
L. Burris
F. A. Cafasso
A. A. Chilenskas
K. Choi
P. Cunningham
D. Day
W. DeLuca
R. Dunne
J. G. Eberhart
R. Elliott
W. R. Frost
E. C. Gay
J. Harmon
F. Hornstra
A. A. Jonke
R. W. Kessie
G. M. Kesser
V. M. Kolba
W. Kremsner
M. L. Kyle
W. W. Lark
S. Lawroski
R. F. Malecha
A. E. Martin
F. J. Martino
C. A. Melendres
A. Melton
W. E. Miller
F. Mrazek
K. M. Myles
T. Olszanski
P. A. Nelson (100)
E. G. Pewitt
E. R. Proud
S. Preto
G. Redding
M. F. Roche
L. E. Ross
M. Saboungi
W. W. Schertz
J. L. Settle
H. Shimotake
J. A. Smaga
R. K. Steunenberg
B. Swaroop
C. A. Swoboda
Z. Tomczuk
R. Varma
D. R. Vissers
S. Vogler
W. J. Walsh
D. S. Webster
S. E. Wood
N. P. Yao
P. Eshman
J. E. A. Graae
J. L. Hamilton
P. A. Eident
T. D. Kaun
J. E. Kincinas
K. Kinoshita
Z. Nagy
K. A. Reed
M. A. Slawecki
N. Otto
C. Sy
A. B. Krisciunas
ANL Contract Copy
ANL Libraries (5)
TIS Files (6)

External:

DOE-TIC, for distribution per UC-94c (182)
Chief, Chicago Patent Group
V. Hummel, DOE-CH
President, Argonne Universities Association
Chemical Engineering Division Review Committee:
R. C. Axtmann, Princeton Univ.
R. E. Balzhiser, Electric Power Research Institute
J. T. Banchero, Univ. Notre Dame
D. L. Douglas, Gould Inc.
P. W. Gilles, Univ. Kansas
R. I. Newman, Allied Chemical Corp.
G. M. Rosenblatt, Pennsylvania State Univ.
J. G. Ahlen, Illinois Legislative Council, Springfield
J. Ambrus, Naval Surface Weapons Center
J. N. Anand, Dow Chemical Co., Walnut Creek, Calif.
F. Anson, California Inst. Technology
P. Auh, Brookhaven National Laboratory
B. S. Baker, Energy Research Corp.
H. Balzan, Tennessee Valley Authority

K. F. Barber, Div. Transportation Energy Conservation, USDOE
H. J. Barger, Jr., U. S. Army MERDC, Fort Belvoir
T. R. Beck, Electrochemical Technology Corp., Seattle
J. A. Belding, Div. Conservation Research & Technology, USDOE
M. Benedict, Massachusetts Institute of Technology
D. N. Bennion, Univ. California, Los Angeles
J. Birk, Electric Power Research Inst.
J. Braunstein, Oak Ridge National Laboratory
M. Breiter, GE Research & Development Center
J. O. Brittain, Northwestern U.
R. Brodd, Parma Technical Center, Union Carbide Corp.
J. J. Brogan, Div. Transportation Energy Conservation, USDOE
E. Brooman, Battelle Memorial Institute, Columbus
B. D. Brummet, McGraw-Edison Co., Bloomfield, NJ
D. M. Bush, Sandia Laboratories
E. Buzzelli, Westinghouse Electric Corp., Pittsburgh
E. J. Cairns, General Motors Research Lab., Warren, Mich.
E. Carr, Eagle-Picher Industries, Joplin
P. Carr, Energy Development Associates, Madison Heights, Mich.
Chloride Systems (U. S. A.) Inc., North Haven, Conn.
C. Christenson, Gould Inc.
C. A. Clemons, PPG Industries, Pittsburgh
M. Cohen, Univ. of Chicago
A. R. Cook, Int'l Lead Zinc Research Organization, Inc., New York City
D. R. Craig, Hooker Chemical Corp.
G. Cramer, Southern California Edison, Rosemead
F. M. Delnick, Sandia Labs.
W. Dippold, Div. Transportation Energy Conservation, USDOE
J. Dunning, General Motors Research Lab., Warren, Mich.
P. Eggers, Battelle Memorial Institute, Columbus
M. Eisenberg, Electrochimica Corp.
R. P. Epple, Div. Physical Research, USDOE
P. L. Fleischner, National Beryllia Corp.
J. H. B. George, Arthur D. Little, Inc.
J. Giner, Tyco Labs., Inc., Waltham, Mass.
C. Goddard, Div. Conservation Research and Technology, USDOE
G. Goodman, Globe-Union, Inc., Milwaukee
G. Gorten, Gorten and Associates, Sherman Oaks, Calif.
H. Grady, Foote Mineral Co., Exton, Pa.
S. Gratch, Birmingham, Mich.
D. Gregory, Institute of Gas Technology, Chicago
N. Gupta, Ford Motor Co.
N. Hackerman, Rice U.
G. Hagey, Div. of Energy Storage Systems, USDOE
C. Halpin, Halpin Engrs. Grosse Point, Mich.
R. Hamilton, Carborundum Co., Niagara Falls
W. Hassenzahl, Los Alamos Scientific Laboratory
L. A. Heredy, Atomics International
B. Higgins, Eagle-Picher Industries, Joplin
R. Hudson, Eagle-Picher Industries, Joplin
J. R. Huff, U. S. Army Mobility Equipment R&D Center, Fort Belvoir
R. A. Huggins, Stanford U.
R. A. Huse, Public Service Electric & Gas Co., Newark, N.J.
S. D. James, U. S. Naval Surface Weapons Center

M. A. Jansen, Allegheny Power Service Corp., Greensburgh, Pa.
G. Janz, Rensselaer Polytechnic Inst.
H. Jensen, C&D Batteries, Plymouth Meeting, Pa.
F. Kalhammer, Electric Power Research Institute
K. Kinsman, Ford Motor Co.
R. Kirk, Div. Conservation Research & Technology, USDOE
K. W. Klunder, Div. of Energy Storage Systems, USDOE
J. Lagowski, Detroit Edison Utility Co.
J. J. Lander, Air Force Aero Propulsion Lab., Wright-Patterson AFB
A. Landgrebe, Div. of Energy Storage Systems, USDOE (6)
C. E. Larson, Bethesda, Md.
S. H. Law, Northeast Utilities, Hartford, Conn.
H. Leribaux, Texas A&M U.
D. Linden, U. S. Army Electronics Command, Fort Monmouth, N.J.
R. Llewellyn, Indiana State U.
P. S. Lykoudis, Purdue Univ.
C. J. Major, PPG Industries, Inc.
G. Mamantov, U. Tennessee
J. Mathers, U. Maryland
C. J. Mazar, PPG Industries, Corpus Christi
J. McKeown, Office of Program Administration, USDOE
C. McMurty, Carborundum Co., Niagara Falls
R. McRae, ILC Technology, Sunnyvale, Calif.
D. Meighan, C&D Batteries, Plymouth Meeting, Pa.
R. Minck, Ford Motor Co.
F. Moore, Div. of Energy Storage Systems, USDOE
G. Murray, Detroit Edison Utility Co.
E. Nicholson, Esso Research & Engineering Corporate Res. Lab., Linden, N.J.
C. Pax, Div. Transportation Energy Conservation, USDOE
G. F. Pezdirtz, Div. of Energy Storage Systems, USDOE
R. Rightmire, Standard Oil of Ohio, Cleveland
R. Rizzo, Globe-Union, Inc., Milwaukee
N. Rosenberg, Transportation Systems Center, Cambridge, Mass.
N. W. Rosenblatt, E. I. duPont de Nemours & Co., Wilmington
R. Rubischko, Gould Inc.
A. Salkind, ESB Inc., Yardley, Pa.
G. Scharbach, American Motors General Corp., Wayne, Mich.
T. Schneider, Public Service Electric & Gas Co., Newark, N.J.
R. I. Schoen, National Science Foundation
J. R. Schorr, Battelle Memorial Institute, Columbus
D. R. Schramm, Public Service Electric & Gas Co., Newark, N.J.
H. J. Schwartz, NASA Lewis Research Center
J. R. Selman, Illinois Institute of Technology
A. I. Snow, Atlantic Richfield Co., Harvey, Ill.
S. Srinivasan, Brookhaven National Laboratory
D. Stakem, Catalyst Research Corp., Baltimore
E. Steeve, Commonwealth Edison Co., Chicago
R. H. Strange II, National Science Foundation
R. L. Strombotne, U. S. Dept. Transportation, Washington
S. Sudar, Atomics International
R. H. Swoyer, Pennsylvania Power and Light Co., Allentown
F. Tepper, Catalyst Research Corp., Baltimore
L. Thaller, NASA Lewis Research Center
G. M. Thur, Div. Transportation Energy Conservation, USDOE

C. W. Tobias, U. California, Berkeley
L. Topper, National Science Foundation
W. Towle, Globe-Union, Inc., Milwaukee
J. Vanderryn, Office of Intern. R&D Programs, USDOE
J. V. Vinciguerra, Eagle-Picher Industries, Joplin
R. D. Walker, Jr., U. Florida
C. O. Wanvig, Jr., Globe-Union, Inc., Milwaukee
S. A. Weiner, Ford Motor Co.
J. Werth, ESB Inc., Yardley, Pa.
C. Wienlein, Globe-Union, Inc., Milwaukee
F. Will, General Electric R&D Center, Schenectady
J. Withrow, Chrysler Corp., Detroit
W. L. Wonell, U. of California, Berkeley
S. Wood, La Grange Park, Ill.
T. Wydeven, NASA Ames Research Center
O. Zimmerman, Portland General Electric Co., Portland, Ore.
M. Zlotnick, Div. Conservation Research and Technology, USDOE
Chloride Technical Limited, Manchester, England
E. Voss, Varta Batterie A.G., Kelkhern, Germany
E. Aiello, U. of Chicago
W. J. Argersinger, Jr., U. of Kansas
J. T. Banchero, U. of Notre Dame
K. J. Bell, Oklahoma State U.
R. Blanco, Oak Ridge Nat. Lab.
C. F. Bonilla, Columbia U.
W. Brandt, U. of Wisconsin-Milwaukee
A. E. Dukler, U. of Houston
W. J. Frea, Michigan Tech. U.
C. D. Harrington, Douglas United Nuclear, Inc.
J. E. Linehan, Marquette U.
Maine Univ., Prof. in charge of Chem. Engr. Lib.
Marquette U., Dept. of Chemistry
Michigan Tech. U., Library
G. Murphy, Iowa State U.
E. A. Peretti, U. of Notre Dame
G. W. Preckshot, Engr. U. of Missouri
H. Rosson, U. of Kansas
C. Sanathanan, U. of Illinois-Chicago Circle
A. Sesonske, Purdue U.
USDOE, Director, Div. of Safeguards and Security
B. W. Wilkinson, Michigan State U.
Comision Nacional de Energia Atomica, Library, Argentina
J. A. Sabato, Com. Nac. de Energia Atomica, Buenos Aires, Argentina
C. H. Cheng, Nat'l Tsing Hau Univ., China
National Radiological Protection Board, Library, Harwell, England
L. Kemmerich, Ges. fur Kernforschung, Karlsruhe, Germany
F. Weigel, Inst. fur Anorganische Chemie der U. Munich, Germany
N. Saratchandran, Bhabha Atomic Research Centre, Bombay, India
K. Fujimiya, U. of Tokyo, Japan
Japan Atomic Energy Research Inst., Tokai-mura, Japan
K. Matsuda, Inst. of Physical & Chemical Res., Yamato-machi, Japan
Sang-Soo Lee, Korea Advanced Institute of Science, Korea
Korean Atomic Energy Research Institute, Korea
Ragnar Nordberg, Sahlgren's Hospital, Goteborg, Sweden

☆ U.S. GOVERNMENT PRINTING OFFICE: 1977 750–133